Numerical aspects of searching convective/absolute instability transition

Sergey A. Suslov

Department of Mathematics and Computing, University of Southern Queensland, Queensland 4350, Australia

Abstract

An overview of various numerical techniques used to determine the spatio-temporal character of instabilities in fluid flows is given. The advantageous features of various previously known individual techniques are discussed and a practical procedure combining them is suggested for a specific task of determining the complete boundary between linearly convectively and absolutely unstable regimes in a multi-parameter space in problems with a fully numerical dispersion relation. Special attention is paid to aspects of automatization of computations as this is a crucial condition for their efficiency. The suggested procedure is successfully used and is shown to provide a high degree of automatism in the physical example of non-Boussinesq mixed convection in a vertical channel. This example comprises most of the major numerical difficulties found in various spatio-temporal instability studies of two-dimensional fluid flows which previously could not be handled without frequent human intervention and visual inspection of intermediate results. This paper focuses on the general numerical aspects of the computations leaving the detailed discussion of the obtained physical results for a separate publication.

Key words: Convective/absolute instability transition, eigenvalue tracking
PACS: 47.32, 47.20, 47.11, 03.40.G, 47.60

1 Introduction

Spatio-temporal convective and absolute instabilities in fluid flows have received increased attention because of their relevance to flow control [1,2] and, ultimately, transition to turbulence [3]. These concepts relate to the asymptotic behavior at large time of an initially localized disturbance envelope. If

Email address: ssuslov@usq.edu.au (Sergey A. Suslov).

this disturbance decays with time everywhere then the flow is referred to as absolutely stable. If it grows when observed with respect to some steadily moving coordinate system, but decay at any stationary location then such a flow is called convectively unstable. Finally, if the growing disturbance is observed at a stationary frame the instability is referred to as absolute. Equivalently, the instability is absolute if the edges of the localized disturbance envelope with growing amplitude move in the opposite directions when considered with respect to a stationary coordinate system, and it is convective if the edges move in the same direction. The distinction between convective and absolute instabilities is well defined only when the Galilean symmetry with respect to uniform translation of a coordinate system is broken so that the stationary (sometimes also called laboratory) system can be distinguished from the others. In this paper we assume that the Galilean symmetry is broken by the no-slip boundary conditions for viscous fluid: the frame with respect to which solid walls limiting the flow have zero velocity is taken to be stationary. Therefore if the asymptotic instability resulting from the initially localized disturbance is observed at any point which is stationary with respect to this system we will refer to this situation as absolutely unstable.

The character of instability is determined by the properties of a complex dispersion relation corresponding to a particular flow. The complete theoretical background of linear convective and absolute instabilities as applied to fluid flows can be found in earlier literature [1,4–6] and here we only introduce definitions and concepts relevant from the numerical point of view. An essential part of this investigation is the asymptotic analysis of the Fourier integrals arising in a formal solution of linearized equations describing evolution of infinitesimal disturbances. Such asymptotic analysis typically involves applications of the Briggs' [7] or steepest descent methods which, if used consistently, lead to identical results [8]. Although well understood by now, both of these techniques require a thorough implementation in order to guarantee the validity of conclusions made about the character of instability in each individual flow situation [5]. This inevitably involves investigation of a global topography of the disturbance complex amplification rate $\sigma = \sigma^R + \mathrm{i}\sigma^I$ over the space of a complex wavenumber $\alpha = \alpha^R + \mathrm{i}\alpha^I$ which are related through the problem's dispersion relation $D(\sigma, \alpha) = 0$. [1]

When the dispersion relation is resolved with respect to $\sigma = \sigma(\alpha)$ for real α the analysis is called temporal. Usually, the dispersion relation is multivalued and therefore multiple images of the real α axis are obtained. Consistent with

[1] Using the amplification rate σ instead of complex frequency $\omega = \mathrm{i}\sigma$ in the context of spatio-temporal instabilities is somewhat unconventional. We are doing this in order to be consistent with notation adopted in earlier publications [9,10] discussing the stability of non-Boussinesq mixed convection flow which will provide most of physical examples in the present work.

definitions given in [4], we will call them temporal branches of the dispersion relation. However for convenience of presentation we will call images of any straight line path in the complex wavenumber plane given by $\alpha^I = a$, where a is an arbitrary ($a \neq 0$ in general) real number, temporal branches $\sigma_i(\alpha)$, $i = 1, 2, \ldots$ as well.

Similarly, if the dispersion relation is resolved with respect to $\alpha = \alpha(\sigma)$ and σ is taken to be imaginary (i.e. real disturbance frequency) the analysis is called spatial. We will call images of any straight line $\sigma^R = b$ in the complex σ plane, where b is an arbitrary real number, spatial contours or spatial branches of the dispersion relation $\alpha_i(\sigma)$, $i = 1, 2, \ldots$. Intersection of the spatial contours (branches) in the complex wavenumber plane at $\alpha = \alpha_s$ will be called a spatial branch point. Although general theory is not restricted to collision of two spatial branches only, this is the most common situation. In this case

$$\left.\frac{\partial \sigma}{\partial \alpha}\right|_{\alpha=\alpha_s} = 0\,, \qquad \left.\frac{\partial^2 \sigma}{\partial \alpha^2}\right|_{\alpha=\alpha_s} \neq 0 \tag{1}$$

and α_s is the saddle point of the second order of the surface $\sigma(\alpha)$. It is formed by intersecting level curves $\sigma^R = \sigma_s^R$ or $\sigma^I = \sigma_s^I$, where $\sigma_s^R = \sigma^R(\alpha_s)$ is the absolute amplification rate, $\omega_s^R = -\sigma_s^I = -\sigma^I(\alpha_s)$ is the absolute frequency and the saddle point wavenumber α_s is called absolute wavenumber. The necessary condition for absolute instability is $\sigma_s^R > 0$, but according to the Briggs criterion [7] it is not sufficient unless the saddle point is the genuine pinch point formed by the spatial branches originating in different (upper and lower) halves of the complex α plane for sufficiently large values of b. Even in the topologically simplest case when a physical flow is two-dimensional and unbounded and uniform in one spatial direction, the search for pinch points is computationally very expensive as noted, for example, in [2], [3] and [11].

As mentioned above, the theory of spatio-temporal instabilities requires very careful consideration of the global topography associated with the complex dispersion relation on a case-by-case basis. For example, when investigating the instability character of a boundary layer flow Lingwood [8] dedicates twelve pages of discussion to determine it rigorously at a single set of physical governing parameters. Accurate computation of a complete convective/absolute instability boundary (CAIB) in a multi-parameter space of a realistic physical problem may require up to several thousands of such points and therefore is a very challenging numerical task. As a consequence although the number of relevant publications has been growing rapidly in the past years (see short review in Section 2), papers presenting CAIBs are generally restricted to relatively narrow ranges of physical parameters over which the transition has been detected (see, for example, [2,3,12–19]).

Apart from the well known difficulty of considering the global $\sigma(\alpha)$-topography, another technical problem arises when CAIB lies sufficiently far away from the

linear instability boundary as, for example, in systems with a relatively strong through-flow. In this case the saddle points of a dispersion relation may be located far away from the real α axis. The temporal stability analysis still identifies the temporally unstable branches $\sigma^R\big|_{\alpha^I=0} > 0$ reliably, but distinguishing the saddle points corresponding to these branches from those of stable ones in a complex wavenumber plane becomes a very challenging task. This is so because the dispersion relation is known only numerically. While the theory takes the fact that its roots can be easily distinguished and tracked for granted, this is rarely the case in practice. The roots of the dispersion relation are only known as a relatively large set of discrete eigenvalues of the linearized problem and it is not clear which one of the eigenvalues leads to the required saddle point when a wavenumber changes in the complex plane. The eigenvalue ordering enforced by a particular numerical solver is typically different for real and complex values of wavenumber α and is not known a priori. As a consequence, many previous investigations have been limited to flows for which the order of leading eigenvalues between the real α axis and a saddle point either does not change [3,11,13,17,20] or is known analytically [14,18]. Because of the computational complexity, very rarely has the attempt been made to analyze the saddle points formed by all leading branches and then to choose only the relevant ones [12,21]. Recently, the aspect of eigenvalue identification has been addressed in [10]. The author showed that the problem of tracking the required branch of a numerical dispersion relation (NDR) might become so severe that reliable computations of CAIB would not be possible (see also [16]). Consequently, one of the major goals of this work is to suggest a procedure enabling automatic identification of the branches of NDR.

Section 2 reviews a large number of recent numerical spatio-temporal instability studies. The list of references is far from complete, yet the review provides a clear idea of contemporary views on numerical aspects of spatio-temporal analysis. Despite the ever-growing interest to spatio-temporal instability studies, to the best of the author's knowledge, a comparative analysis of used numerical techniques has not been presented in literature to date: relevant knowledge remains scattered across dozens of individual papers. Therefore bringing this knowledge together in a usabale compact form is another major goal of this paper. Common difficulties are identified and the efficient ways of resolving them are discussed. In the light of this review a more automated computational procedure emerges that combines the most efficient elements of previously known techniques with a more reliable tracking of the branches of NDR. Such a procedure is discussed in Section 3. Since the suggested procedure is based on selected elements of the techniques developed elsewhere the reader is referred to the original works for rigorous proofs of their validity. Their qualitative interpretations are used here to explain the improved performance of the combined procedure designed specifically for searching convective/absolute instability transition. However a few instances where no complete theory is yet available to rigorously justify the proposed steps are

flagged in Section 3.3. In these cases the success of the suggested procedure is demonstrated in a particular example and qualitative conjectures are given explaining this success.

This work was initially motivated by the author's research of spatio-temporal instabilities arising in mixed convection flows of non-Boussinesq fluid. None of the individual techniques previously reported in literature were able to overcome all the numerical difficulties encountered in CAIB computations for such flows efficiently. Therefore the procedure presented in this paper was developed and was successfully applied to produce the required physical results. These computations provided most of the illustrative examples in the current paper. The physical set up and governing equations for this example problem are given in [9]. In brief, the undisturbed two-dimensional parallel flow whose stability is investigated is driven by the pressure gradient applied along the channel and by the buoyancy force caused by the nonlinear density variation due to the cross-channel temperature gradient. The flow is governed by four major physical parameters: the Reynolds number Re, the Grashof number Gr, the Prandtl number Pr and the non-dimensional temperature difference ϵ between the walls which characterize the applied pressure gradient, the buoyancy force, the relative importance of thermal and viscous forces and the degree of nonlinearity of the fluid's transport properties, respectively. In the discussed example, the Prandtl number is fixed to 0.71 while the rest of the governing parameters are chosen to illustrate clearly the most general difficulties arising in computations related to spatio-temporal stability analysis. The corresponding linear disturbance problem was formulated, and comprehensive temporal stability analysis was performed in [9] and selected spatio-temporal instability results obtained using the current algorithm were reported in [22–24]. For this reason only the resulting NDR (2) has been used here. The suggested procedure for searching CAIB is shown to cope well with many technical difficulties associated with the complexity of this problem's NDR such as the presence of multiple physical instability modes and multiple saddle points. The procedure is also offers a higher degree of automatization than that achieved in similar computations before. This enabled the author to obtain a rich spectrum of remarkable physical results concerning the nature of instabilities in non-Boussinesq mixed convection for a very wide range of governing physical parameters. Nevertheless here we focus only on the numerical aspects of the analysis. The comprehensive physical interpretation of the results will be the subject of a separate full length publication.

Finally, the example used here is concerned with two-dimensional flow with one unbounded direction ($[x, y] = [0, 1] \times (-\infty, \infty)$). Upon applying the Fourier transform in this direction the dispersion relation which depends on a single wavenumber is obtained. Thus the complete numerical procedure is developed for this situation. Many of the major steps of the algorithm can be generalized for three-dimensional flows with two unbounded directions as those considered

in [17,25–27]. Yet three-dimensional flows offer a much wider variety of situations which may result in technical difficulties not present in two-dimensional studies and therefore not discussed in the current paper. It might or might not be possible to develop a reliable fully automatic algorithm for searching convective/absolute instability transition in three-dimensional flows. However the answer to this question is presently unclear and should, perhaps, be attempted after a much larger number of three-dimensional studies is completed than that reported in literature to date in order to form a firm ground for the required case study.

2 Brief overview of numerical procedures

Analysis of the nature of spatio-temporal instability includes a number of steps each involving a significant numerical component. Firstly, the original physical problem is linearized about some known (basic) solution and the corresponding dispersion relation between the complex amplification rate of infinitesimal disturbances and their complex wavenumber is established as the function of the physical governing parameters. Except rare cases when the basic solution is simple and known analytically [14,15,18] such a dispersion relation can only be obtained numerically due to the complexity of the physical problem [3,28] using temporal or spatial linear stability analyses. Both types of analyses lead to identical conclusions about the linear instability of a basic solution, but their numerical implementation differs significantly. This difference stems out from the fact that the original governing partial differential equations (such as the Navier-Stokes equations) are first order in time and at least second order in space. Because of this, the Fourier transforms of the disturbance equations result in nonlinear (at least quadratic) terms in wavenumber while the temporal amplification rate enters them linearly. Consequently, temporal stability analysis results in a linear eigenvalue problem for the disturbance amplification rate while its spatial counterpart always leads to a nonlinear eigenvalue problem for the disturbance wavenumber.

Both types of eigenvalue problems can be accurately solved using the shooting technique. This approach was successfully used in a number of spatio-temporal instability studies [12,13,16,18,28]. Nevertheless such approach has two major disadvantages. First, finding each eigenvalue requires full integration of the linearized disturbance equations. This might become a challenging task on its own especially when integration has to be performed along the path in a complex plane and analyticity properties of the solution have to be checked thoroughly. This was required, for example, in [16]. The computational cost of finding eigenvalues in such a way is high and the method might become impractical if the global stability picture in a multi-parameter space is sought. Another serious drawback is that the shooting technique requires a reasonably

accurate initial guess in order to converge to a necessary eigenvalue. For example, previously known results from temporal stability studies [29] and direct numerical simulation results from [30] had to be used in [16] to find spatial eigenvalues by the shooting method. In another example Krizhevsky *et al.* [13] resorted to tracing the argument of a complex function corresponding to the dispersion relation along a sequence of closed contours in the α plane in order to determine the initial guess. In general, the information about the eigenvalue spectrum is not known a priori and thus a reliable application of the shooting method might become difficult. This method fails completely when the eigenvalue spectrum is dense because then the shooting procedure jumps from one eigenvalue to another as was observed in [16] and convergence cannot be achieved.

Alternatively, a set of *all* leading eigenvalues can be computed in a single run if the disturbance equations are discretised and written as a matrix eigenvalue problem. In contrast to a shooting method where the efficiency and accuracy of computations depend strongly on the availability of a reliable initial guess and the implementation of the integration algorithm [16], solution of the algebraic eigenvalue problem is a generic procedure [3,11] whose highly optimized implementations are readily available in various professional mathematical libraries (e.g. IMSL, NAG, LAPACK) and for various computer architectures including parallel. The only drawback of this approach is that it might produce spurious eigenvalues resulting from the specifics of a discretization method used to approximate the equations and the boundary conditions. Fortunately, the spurious eigenvalues are relatively easy to detect because of their strong dependence on the discretization parameters. For example, recomputing the eigenvalue spectrum with an extra grid point leaves physical eigenvalues practically unchanged while spurious eigenvalues change by more than an order of magnitude. Since solving a linear algebraic eigenvalue problem is a routine task, and efficiency of the existing standard algorithms is sufficiently high, filtering the spurious eigenvalues out by recomputing the problem with slightly changed discretization parameters has become a common practice in stability analyses, see for example [19,21].

As has been mentioned previously, in the case of temporal instability analysis, the linearisation and discretization of the Navier-Stokes-type equations leads to an algebraic eigenvalue problem of the form

$$\mathbf{A}\boldsymbol{w} = \sigma\mathbf{B}\boldsymbol{w}\,, \tag{2}$$

where $\mathbf{A}$ and $\mathbf{B}$ are matrix operators resulting from discretization of the governing equations, $\boldsymbol{w}$ is the disturbance eigen-solution and the eigenvalue $\sigma = -\mathrm{i}\omega$ is the complex amplification rate (ω is the complex frequency). Operators $\mathbf{A}$ and $\mathbf{B}$ in general are nonlinear functions of physical parameters and wavenumber α. Depending on the boundary conditions, the nonlinearity in

wavenumber can be high order polynomial [31,32] or even transcendental as in an example considered in [4]. When the physical parameters and wavenumber are fixed, equation (2) represents a linear generalized matrix eigenvalue problem which can be solved using standard computational algorithms (e.g. QZ).

The situation is more complicated in the case of spatial stability analysis. Even in the simplest viscous flow situation the matrix eigenvalue problem resulting from the linearized Navier-Stokes equations written in primitive variables is quadratic in wavenumber α

$$\mathbf{C}\boldsymbol{w} = \alpha\mathbf{D}\boldsymbol{w} + \alpha^2\mathbf{E}\boldsymbol{w}\,. \tag{3}$$

It is typically solved using the companion matrix technique [3,11,19,21,33,34] in which the nonlinear eigenvalue problem is linearized by augmenting the eigenvector to $\boldsymbol{w}' = (\boldsymbol{w}, \alpha\boldsymbol{w})^T$ so that the problem becomes a standard one

$$\begin{pmatrix} \mathbf{C} & \mathbf{0} \\ \mathbf{0} & \mathbf{I} \end{pmatrix} \begin{pmatrix} \boldsymbol{w} \\ \alpha\boldsymbol{w} \end{pmatrix} = \alpha \begin{pmatrix} \mathbf{D} & \mathbf{E} \\ \mathbf{I} & \mathbf{0} \end{pmatrix} \begin{pmatrix} \boldsymbol{w} \\ \alpha\boldsymbol{w} \end{pmatrix}\,, \tag{4}$$

where $\mathbf{I}$ is the identity matrix. The obvious disadvantage of such an approach is that the size of the problem essentially doubles. As a result the computational cost and the number of spurious eigenvalues increases substantially in comparison with the similar problem (2) arising in temporal stability analysis. For this reason it is advantageous to perform numerical spatio-temporal instability analysis based on temporal instability calculations i.e. for the dispersion relation of the form $\sigma = \sigma(\alpha)$ rather than $\alpha = \alpha(\sigma)$ (see [4,35,31,26,27]). This is especially so when the complete CAIB in multi-parameter space including several hundreds of individual points is required or when the dispersion relation is transcendental in α so that the companion matrix technique is not applicable [4].

Once the problem's NDR is established by using one of the techniques described above, the convective or absolute nature of instability is determined in two major steps. The first is locating the spatial branch point (or, equivalently, the temporal saddle point) α_s of the dispersion relation in a complex wavenumber plane at which equations (1) are satisfied and examine the absolute growth rate $\sigma^R(\alpha_s)$ ($\sigma^R(\alpha_s) < 0$ means stability or convective instability, $\sigma^R(\alpha_s) > 0$ may correspond to absolute instability). The second important step is checking if the so-called pinching condition is satisfied for this saddle point, see [7,6].

This may be done in a number of ways. The method which follows directly from Briggs [7] theory which is summarized in [6] in the context of fluid flows essentially uses an approach based on the spatial analysis. It initially fixes $\sigma^R = \sigma_0^R$, where $\sigma_0^R > \max_{\alpha^I=0}\left(\sigma^R(\alpha)\right)$. This corresponds to a vertical line in

a complex σ-plane. Then the multiple images (spatial contours) of this path are found in the complex wavenumber space using shooting or companion matrix technique. As the value of σ^R is gradually decreased (by translating the initial vertical line $\sigma^R = \sigma_0^R$ towards $\sigma^R = 0$) the corresponding images in a wavenumber plane approach each other and eventually collide forming a spatial branch point where $\frac{\partial \sigma}{\partial \alpha} = 0$ (saddle point of the $\sigma(\alpha)$ surface). As discussed in [7,6] if the two colliding contours originate in different halves of the α-plane then they correspond to downstream and upstream spatial instabilities. Their collision means that in such a regime instability will be observed in both directions (i.e. will be absolute) provided that the absolute amplification rate $\sigma^R(\alpha_s) > 0$. If collision occurs between the spatial branches originating in the same half of the α plane then spatial instability is observed either upstream or downstream and the spatio-temporal instability can only be convective.

While topographically straightforward, this approach relies in large measure on the efficiency of solving the problem dispersion relation with respect to wavenumber α for a fixed complex amplification rate σ [16,21]. As has been discussed above, it is computationally more expensive and less convenient than finding σ as a function of α. Besides locating the branch point, this approach requires identifying and tracking the colliding spatial branches. This has been done by computing and plotting a set of contour lines $\sigma^R = \text{const.}$ over the complex wavenumber plane with subsequent visual analysis of the obtained global picture [13,18]. Thus the procedure involves an essential interactive component which makes it somewhat subjective and inefficient because the computational process is not fully automatic.

Since the branch points of the spatial dispersion relation $\alpha(\sigma)$ correspond to the saddle points of the temporal dispersion relation $\sigma(\alpha)$, a number of spatio-temporal instability studies have used criterion (1) to locate the branch (saddle) points and then determine the character of the instabilities. Checking this criterion involves computing the temporal amplification rate as a function of the wavenumber which is generally more convenient than tracking the spatial branches in the approach described above. The actual location of the saddle point can be found iteratively using Newton-type methods to find the root of equation (1) [2,16,17,36]. Such an approach is accurate and efficient because of the relatively quick convergence. It is essentially local in its nature as it only requires the values of σ in the vicinity of a current point to approximate the local derivatives and form a Jacobian used by Newton iterations. It does not require visual control of the intermediate results because checking the zero derivative condition can be done automatically within a numerical code. Nevertheless this method has its own problems. Firstly, the convergence of iterations might be slow or the method might even diverge if the initial guess is chosen far away from the saddle point. To overcome this difficulty Yin *et al.* [2] and Krizhevsky *et al.* [13] had to determine an initial guess from a

visual inspection of the ω (σ in our notation) contours on a coarse grid in complex wavenumber plane. Secondly, the analytical expression for $\sigma(\alpha)$ is rarely known so that the dispersion relation and its derivatives must be approximated numerically, say, using finite differences. Application of Newton-type iterations to find zero of a derivative necessarily involves the Jacobian formed by the second derivatives which also have to be approximated numerically. This makes an iterative search of a saddle point vulnerable to any singularities of the dispersion relation. A typical example of singularity associated with "colliding" (multiple) eigenvalues of the linearized problem will be considered in detail in Section 3. Lastly, while the locality of the method is an advantage at the stage of the iterative search, the procedure does not guarantee that the found saddle point satisfies the pinching condition, i.e. that it is formed by spatial branches originating in different halves of the wavenumber plane. In fact, many of the saddle points of the dispersion relation may not be pinch points and may not determine transition to absolute instability. For example, an infinite number of saddle points were found in the studies of Eady model by [5] and none of them contributed to absolute instability. A similar situation was detected in [12] for axisymmetric jets and in [28] for mixed convection boundary layers. Therefore the relevance of a computed saddle point to absolute instability is a very delicate issue for most physical flows. In order to verify that the saddle point is a pinch point one has to reconstruct the complete $\sigma(\alpha)$ surface around the saddle point and check that the $\sigma^R(\alpha)$ =const. contour lines (spatial branches of the dispersion relation) forming the saddle point belong to the different halves of the complex α plane for sufficiently large values of σ^R [12,37]. This is computationally a very demanding procedure. For this reason, frequently the global pinching condition is checked only for a selected set of parameters assuming that the topography remains qualitatively the same for a complete parameter range [17]. Besides that, the analysis of the so-obtained global picture has to be done visually [14–16,19,21,28] which prevents full automatization of computations.

A different procedure which allows checking the pinching criterion has been suggested by Kupfer *et al.* [4]. After realizing that in many physical problems it is easier to compute σ as a function of α they developed a method of locating the pinch points by mapping from the α into σ plane. The computational scenario in this case is very similar to that of a temporal instability analysis. Namely, the imaginary part of the wavenumber, α^I, is kept fixed while σ is computed for a range of α^R. Then the corresponding image in the σ plane is constructed. It has been shown that the branch (saddle) point of a dispersion relation corresponds to a cusp singularity of the image of the α^I =const. contour in the σ plane. Thus the saddle point is found by varying α^I and inspecting the image in the σ plane until the cusp formation is detected. Unfortunately, it is difficult to do this accurately because the decision whether the cusp has been formed has to be made based on a visual inspection of the map [3,11,27]. Consequently, the resulting conclusion is somewhat sub-

jective and cannot be made without human intervention. For this reason the procedure suggested in [4] seems to have little advantage over the automatic saddle point search using the iterative procedure outlined above. In fact, Yeo *et al.* [11] had to use the "zero group-velocity" criterion $\frac{\partial \omega}{\partial \alpha} = 0$ in order to find the branch point accurately after it has been roughly estimated using the cusp criterion. On the other hand, the procedure of Kupfer *et al.* [4] offers a computationally inexpensive way of checking whether the found saddle point is a pinch point without constructing a global picture. Once the saddle point α_s (and thus the cusp point) is located, a set of eigenvalues of a linearized problem are computed for real wavenumbers: $\sigma_{0j} = \sigma_j(\alpha)|_{\alpha^I=0}$, $j = 1, 2, \ldots$. Then according to the arguments developed in [4] one only has to count the number of times the cusp point in the σ plane is covered by the images of σ_{0i}. The cusp corresponds to a pinch point only if it is covered an odd number of times (most common situation corresponds to a cusp point covered once, see, for example, [3,11]).[2] Apart from the low cost of such computations the procedure can be made fully automatic as the analysis is essentially reduced to checking the values of σ_{0j}^R for σ_{0j}^I equal to that at a saddle point. This is discussed in detail in Section 3.2.

As seen from the above review, although a general theory of convective and absolute instabilities is nowadays well understood, determining a complete transition boundary between convective and absolute instabilities remains a challenging computational task. Researchers have had to rely on their experience in developing individual numerical approaches for each problem studied. The major difficulty adversely affecting the efficiency of such computations is associated with a necessity of subjective visual inspection of the results by a human. In Section 3 we discuss an algorithm which combines the advantageous features of several previously known approaches with an eigenvalue tracking procedure which enables a significantly higher degree of automatization than in the studies reported to date.

[2] As noted by the referee there exists a theoretical possibility for this procedure to fail if $\sigma(\alpha_1) = \sigma(\alpha_2)$ for real $\alpha_1 \neq \alpha_2$ and $\sigma^R(\alpha_1) = \sigma^R(\alpha_2) > 0$. Then it is possible that the cusp covered an odd number of times would not correspond to a pinch point. However even if such a situation is possible in principle it has not been reported in physical flow studies to date. Therefore it is believed that it could occur only at isolated points of the physical parameter space and therefore it would not have a significant impact on the shape of complete CAIB in a multi-parameter space whose computation is the major emphasis of this work.

3 Numerical search of convective/absolute instability boundary

3.1 Saddle point search and Riemann sheet tracking

As follows from discussion in Section 2 the core of the spatio-temporal instability consideration is the analysis of the problem's numerical dispersion relation. Upon discretization of disturbance equations, it is more convenient and numerically advantageous to represent it in a form of a temporal linear generalized eigenvalue problem (2) [4,31] because an equivalent spatial eigenvalue problem is always nonlinear and its solution is computationally more demanding. Initially, all physical governing parameters entering operators $\mathbf{A}$ and $\mathbf{B}$ are fixed to some values and all leading eigenvalues σ are computed using a standard (e.g. *QZ*) algorithm for a range of real wavenumbers α. Theoretically, this range should include all real values of α from minus to plus infinity. In practice though it is often shown that the problem's eigenvalue spectrum is symmetric and only eigenvalues for $\alpha > 0$ need to be computed. It is also possible to prove for some problems that a basic flow is stable for the large values of $\alpha \to \infty$, for example, because of a strong stabilizing influence of surface tension or viscosity on fine flow structures which correspond to large disturbance wavenumbers. Therefore only the range $0 \leq \alpha \leq A$ is treated numerically, where the limit A depends on the problem and is found by gradually increasing α from 0 until all computed σ^R values (after going through their maxima as a function of α) decrease well below zero. If for all examined values of α the amplification rate $\sigma^R < 0$ the flow is linearly stable and no further linear analysis is necessary. Then the physical parameters are changed and the computations are repeated until a regime is found in which there exists a range of α for which $\sigma^R > 0$ (we refer to these eigenvalues as forming a temporally unstable branch of NDR and track them over the complex wavenumber space in further analysis). After that the value of wavenumber α_m is found for which $\sigma_m^R = \max_{\alpha^I=0}\left(\sigma^R(\alpha)\right)$. This procedure corresponds to a standard temporal analysis and can be made fully automatic as it only involves checking the sign and magnitude of σ^R. It requires solving a set of linear matrix eigenvalue problems and hence is computationally straightforward. The spurious eigenvalues, if they appear, are filtered out by recomputing and comparing the eigen-spectrum for slightly changed discretization parameter which is also done automatically (by, say, discarding the eigenvalues whose magnitudes vary by a quantity exceeding a set threshold when a discretization parameter is changed). The values of α_m and σ_m^R are stored for future use. A typical picture is shown in Fig. 1 (a). Note that in general the curve $\sigma^R(\alpha)$ can have multiple maxima as in Fig. 5 or there could be several distinct positive $\sigma^R(\alpha)$ curves, see for example, [38]. In these cases all values of α_m and σ_m^R are stored.

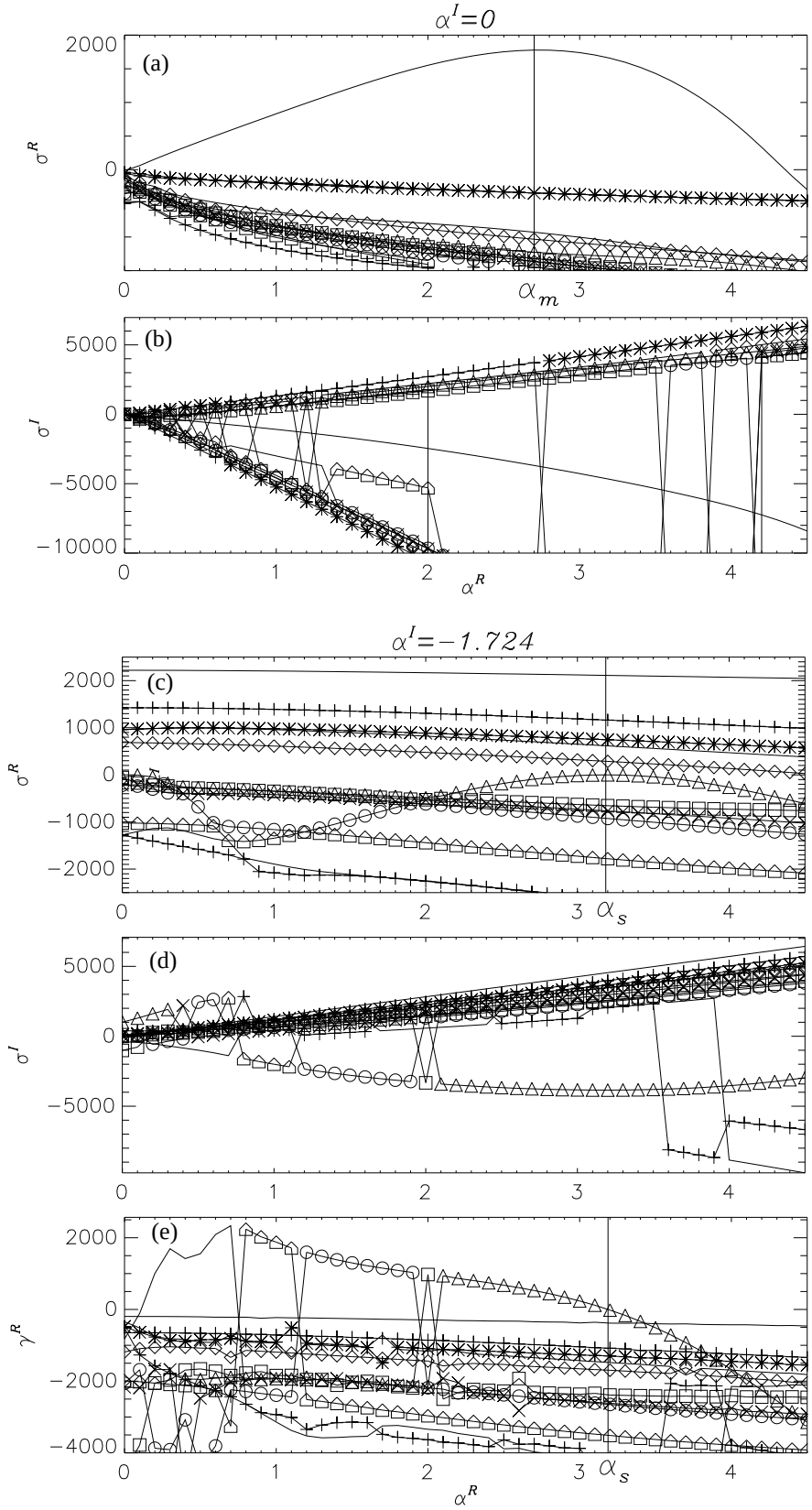

Fig. 1. Temporal branches of NDR and parameter γ^R in the complex wavenumber plane for $(Re, Gr, \epsilon) = (2000, 407705, 0.005)$. Different symbols are used to distinguish between eigenvalues sorted by a numerical code in the descending order of σ^R.

If the results of temporal analysis indicate the presence of unstable modes, i.e. the presence of eigenvalues σ with positive real parts for some range of real wavenumbers α one can proceed to determine the spatio-temporal character of instability. Computationally more efficient way of doing this is via locating saddle points formed by temporally unstable branches i.e. the saddle points which belong to the same Riemann sheets of a dispersion relation as its roots $\sigma(\alpha)$ which have positive real parts for a range of real α. Newton iterations which terminate when $\left|\frac{\partial\sigma}{\partial\alpha}\right|$ becomes sufficiently small offer a fast automatic way of finding the saddle point α_s. Since the analytical expression for a dispersion relation is not known, its derivative can be estimated, for example, via finite difference approximation using the eigenvalues computed at close values of α, or via two-dimensional interpolation formulae as was done, for example, in [2] and [20]. The value of α_m on a real wavenumber axis is a natural starting point for iterations as the spatio-temporal instability analysis has to be performed for a corresponding most unstable branch of NDR (further arguments why this is the preferable starting point will be given later in this section). This resolves the first of the difficulties (choice of the initial guess) with the iterative search for a relevant saddle point.

The second difficulty stems out from the fact that any Newton-type iterations require approximation of a corresponding Jacobian which in this case involves unknown second derivatives of NDR. They also have to be estimated numerically. This might lead to the de-stabilization of iterations and in some cases to their blowup (discussed below). Thus an alternative iterative method which does not require approximating higher order derivatives is necessary. This could be any unconstrained optimization method for minimizing, say,

$$F = \left(\frac{\partial\sigma^R}{\partial\alpha^R}\right)^2 + \left(\frac{\partial\sigma^R}{\partial\alpha^I}\right)^2 . \tag{5}$$

In the example considered here a classical simplex method was used because its implementation was readily available in a standard IMSL routine DUMPOL. Other similar methods (e.g. [39]) could offer a faster convergence, however they might be more sensitive to singularities of NDR and therefore in some severe cases might become less robust than the simplex algorithm. This will be discussed in more detail below. Each simplex iteration requires solving only three eigenvalue problems (2) (at α, $\alpha + \Delta\alpha$ and $\alpha + \mathrm{i}\Delta\alpha$) to evaluate finite difference derivatives entering the functional, while the finite difference approximation of the Jacobian involving second derivatives requires solving five eigenvalue problems. In addition the simplex method is stable in the sense that it is less sensitive to the choice of a starting point. On the other hand it is characterized by slow convergence which might outweigh the computational saving achieved at the derivative approximation stage in comparison with using Newton's method. Besides the minimization procedure may converge to a nonzero local minimum of functional (5). Thus it is suggested to start

the iterative saddle point search using the simplex method and switch to a Newton-type iterations when the value of (5) is reduced to a certain threshold. This hybrid procedure was successfully used in the example computations reported later in this paper.

No matter which method is used for the saddle point search, a severe technical difficulty may occur at this stage which prevented fully automatic computations in previous studies. Its essence is described next.

Any numerical code for eigenvalue calculation returns a set of numbers σ_j, $j = 1, 2, \ldots$. Since only temporally unstable branches of NDR with $\sigma^R > 0$ (for real α) are of interest, it is initially most convenient to arrange the computed eigenvalues in a descending order of the real part $\sigma_1^R > \sigma_2^R > \cdots$. Only a few leading eigenvalues, whose real parts σ_j^R, $j = 1, 2, \ldots, M$ may be positive, define the linear instability and contribute to the asymptotic behavior of the flow. Therefore only the corresponding saddle points α_{sj} have to be considered. The required eigenvalues obtained numerically have to be reliably identified among the others in the due course of iterations over the complex α plane. So far the eigenvalue identification has been done by visual inspection of a global picture [12,13,15]. In some flows the saddle points are located relatively close to the real α line and thus the eigenvalue numbering based on σ^R remains the same as that in temporal stability analysis along the real wavenumber axis. Such situations normally occur when transition to absolute instability is detected in weakly supercritical regimes when CAIB is relatively close to the linear instability boundary in a parameter space, for example, in systems with weak through flow [17,35]. For more complicated flows the eigenvalue numbering based on the size of their real parts becomes misleading. A typical situation is shown in Fig. 1 where different symbols are used to distinguish eigenvalues sorted in the descending order of their real parts. It is clear that only one (temporal) branch σ_1 of NDR contributes to the asymptotic behavior of the flow in this case as only its real part is positive for real wavenumbers as shown by the solid line in the top plot. Therefore it is natural to start a saddle point search by trying to satisfy condition (1) for σ_1. However after a few iterations an iterative (simplex) search algorithm seems to find a local nonzero minimum for (5) and does not make any further progress. Switching to Newton iterations lead to a blowup of the approximated Jacobian and a rapid divergence of further iterations. Inspection of the intermediate results shows that starting from a certain nonzero value of α^I the initially assumed ordering of eigenvalues does not follow the leading temporal branch anymore as the required eigenvalue does not have the largest real part. Attempting to continue using σ_1 in iterations leads to the above problems.

The reason why the σ^R-based ordering fails becomes clear upon considering Fig. 1 (b). The $\sigma_j^I(\alpha)$, $\alpha^I = 0$ curves have slopes $\partial\sigma_j^I/\partial\alpha^R$ of different signs. Therefore according to the Cauchy-Riemann conditions signs of $\partial\sigma_j^R/\partial\alpha^I$ are

also opposite. This means that as one moves away from the real α axis the initially well separated $\sigma_j^R(\alpha)$ values move towards each other, some increasing, some decreasing, and eventually collide.

These "collisions" of a required temporal branch with other branches in complex wavenumber plane are very common and cause a severe technical difficulty [10]. Note that the term "collision" in the context of this study is not used to denote "true" collisions, i.e. temporal branch points where two or more eigenvalues σ have the same complex values at the same complex wavenumber (multiple temporal roots of a dispersion relation). "True" collisions are relatively rare and, if they do occur, require special treatment because a proper branch cut separating the colliding Riemann sheets has to be carefully introduced in this case (see discussion in Section 3.3). The much more common situation discussed here occurs when two eigenvalues have the same real, but different imaginary parts at the same complex wavenumber. This does not cause any difficulty in theory as the two eigenvalues (or the two temporal roots of a dispersion relation) are distinct, but ruins any numerical procedure which uses the eigenvalue sorting based on their real parts. When the saddle point is located far away from the real α axis the number of such "collisions" in the region between the real α axis and a saddle point can be great making an automatic search extremely difficult. In the example of Fig. 1 the first saddle point is found at $\alpha^I = -1.724$. A visual inspection of Fig. 1 (c) shows that only the curve labeled by triangles can pass through a saddle point because, in contrast to others, it has maxima at which derivatives are zero. But this curve represents σ_6, not the leading eigenvalue under the ordering scheme based on the size of σ^R. Moreover it is impossible to confirm that it belongs to the same Riemann sheet of a dispersion relation as the σ_1 curve in the top plot without knowing the full history of "collisions" on the way to the saddle point. Besides, the conclusion that the σ_6 branch is the only candidate to form a saddle point can only be made after inspecting a global picture over a sufficiently wide range of wavenumbers. It appears impossible to make such a conclusion based on the local information when only the values of $\sigma_j(\alpha_s)$ are computed. Consequently, identifying the correct eigenvalue is a key step towards a full automatization of the spatio-temporal analysis. This should be done using appropriate ordering of numerically obtained eigenvalues.

The example of Fig. 1 shows that the σ^R-based sorting fails. Sorting based on the magnitudes or the size of the imaginary parts of eigenvalues does not resolve the problem either as these characteristics are not related to the analytical properties of the problem's dispersion relation. Indeed, the leading eigenvalue (top solid line in Fig. 1 (a)) has the fifth largest imaginary part (solid line in Fig. 1 (b)) while the eigenvalue of interest at $\alpha^I = -1.724$ (line partially marked by triangles in in Fig. 1 (d)) has the eleventh largest imaginary part and therefore sorting based on the size of the imaginary part with the purpose of keeping track of the required eigenvalue is equally unsuccessful.

In some cases it can be possible to resolve the above difficulty by using the two simultaneous eigenvalue ordering systems and switching between them when one of the sorting procedures fails. For example, introduce the notation σ_{kl}, where k is the eigenvalue position in a set sorted by the size of the real part $\sigma_1^R > \sigma_2^R > \cdots > \sigma_k^R > \sigma_{k+1}^R > \cdots$ and l is its position in a set sorted by the size of the imaginary part $\sigma_1^I > \sigma_2^I > \cdots > \sigma_l^I > \sigma_{l+1}^I > \cdots$. Then one starts at a real wavenumber with $\sigma(\alpha_m) = \sigma_{1l}$ (l happened to be 5 in the example of Fig. 1). Initially, it is safe to use the eigenvalue with first subscript $k = 1$. However when moving gradually into the complex wavenumber plane one finds that, at some $\alpha^I \neq 0$, $\sigma_{1l}^R \approx \sigma_{2l'}^R$, $l' \neq l$. Clearly, when the difference $\left|\sigma_{1l}^R - \sigma_{2l'}^R\right|$ becomes sufficiently small, say, less than some small value ϵ, the ordering based on the size of the real part becomes unreliable as the two real parts are about to collide. At the stage when the two real parts are close but still distinguishable the position l of a required eigenvalue in a set sorted by the size of the imaginary part is then detected and the eigenvalue with the second subscript l is used in further computations rather than the eigenvalue with the first subscript 1. Eventually, as the iterative saddle point search progresses beyond the point of the "collision" of real parts the difference between the two leading real parts increases again and from now on eigenvalue σ_{2l} is used in computations until the next "collision" is encountered i.e. until one of the conditions $\left|\sigma_{2l}^R - \sigma_{1l'}^R\right| \leq \epsilon$ or $\left|\sigma_{2l}^R - \sigma_{3l''}^R\right| \leq \epsilon$, $l \neq l' \neq l'' \neq l$ is satisfied. The procedure is repeated until a saddle point is found in the complex wavenumber plane. Clearly, this tracking approach only works if no "true" collisions occur and the iterative increments $\Delta\alpha$ in individual iterations remain sufficiently small and relatively regular so that the switch between the two ordering schemes occurs just before the real part collision. Numerical experiments show though that the latter conditions are difficult to satisfy in practice. The optimal value of tolerance ϵ is not known and the iterative path determined by a specific search algorithm (e.g. simplex or Newton iterations) is frequently irregular and is prone to overshoot the collision points. A typical example of such a path is shown by an irregular solid line in Fig. 3. Regularization of the iterative path by artificially reducing the α increment, although possible to a certain extent, would reduce the convergence rate and therefore the computational efficiency of a saddle point search algorithm.

An even more severe limitation of the above tracking approach was pointed out to the author by Dr D.G. Duffy of NASA/GSFC [40]. He found that the temporal instability of some atmospheric fronts (with reflectional symmetry) is determined by a pair of complex conjugate eigenvalues (at $\alpha^I = 0$) as shown in the two top plots in Fig. 2. Stepping away from the real α axis, say, in the lower half of the complex α plane breaks the symmetry, and the two dominant eigenvalues are not complex conjugate of each other anymore, see the middle two plots in Fig. 2. Yet the readily available information about the magnitudes of the real and imaginary parts of the two leading eigenvalues is insufficient to decide which one of them forms a saddle point and defines the asymptotic

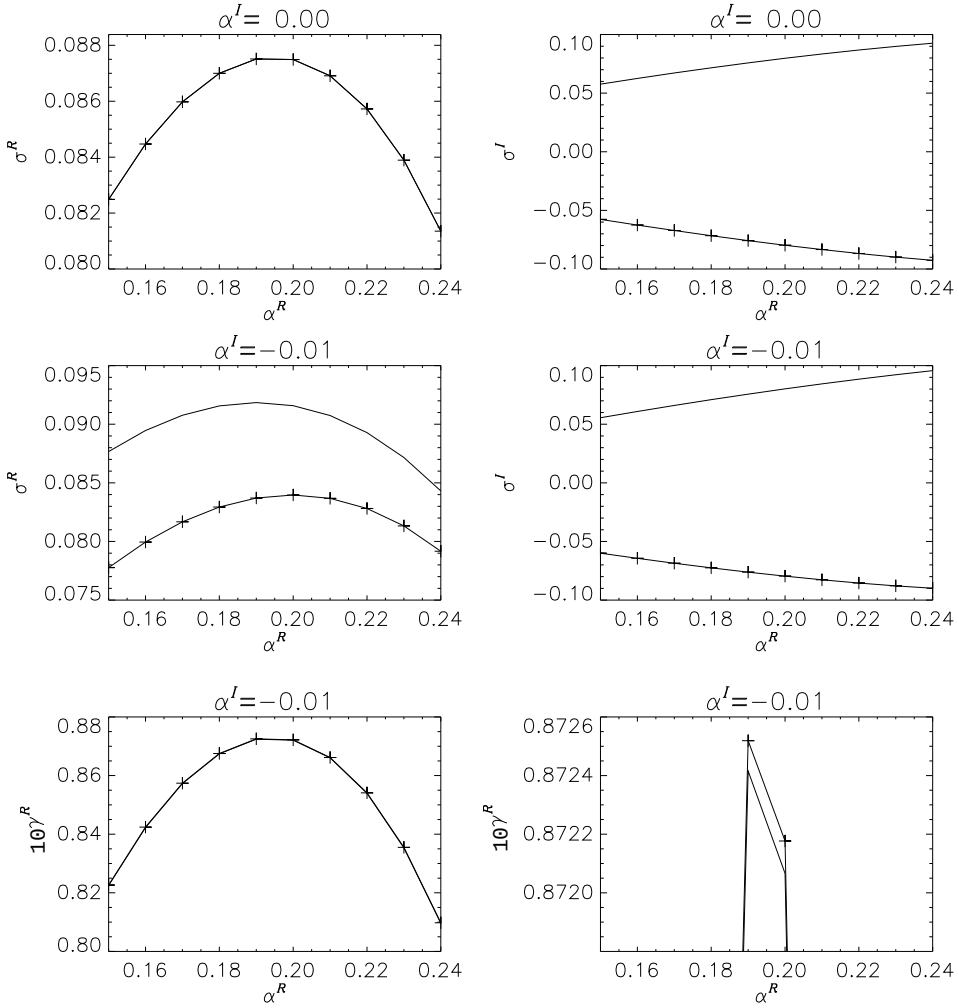

Fig. 2. Temporal branches of NDR and parameter γ^R in the complex wavenumber plane for an example of atmospheric front instability by Dr D.G. Duffy [40]. Different symbols are used to distinguish between eigenvalues sorted by a numerical code in the descending order of σ^R. The bottom right plot is a close-up view of the left plot.

behavior of the system. Additional information is required to proceed with the analysis.

Theoretically, the leading temporal branches should be placed on separate Riemann sheets [4]. The above discussion shows that to do this numerically is a very challenging task which has not been addressed adequately to date. In order not to adversely affect the efficiency of the computational process the procedure must be inexpensive, local in the sense that one should be able to use only quantities obtained at a particular value of α to identify the required eigenvalue, and it should not involve any visual inspection or other sort of human intervention in the due course of the saddle point search.

Such a procedure involving only one eigenvalue ordering system was suggested

by the author in [10]. The core part of the technique is computing quantity

$$\gamma_j^R = \sigma_j^R + \alpha^I \left(\partial\sigma_j^I/\partial\alpha^R\right) = \sigma_j^R - \alpha^I \left(\partial\sigma_j^R/\partial\alpha_j^I\right) \tag{6}$$

along with eigenvalues σ_j (in writing the above equation, the Cauchy-Riemann condition $\partial\sigma_j^R/\partial\alpha^I = -\partial\sigma_j^I/\partial\alpha^R$ was used); then starting from α_m a saddle point is sought for the branch which always corresponds to the largest value of γ_j^R. In brief, the reasons why this numerical recipe works satisfactorily are as follows. If parameter γ^R is computed at the wavenumber for which $\partial\sigma^R/\partial\alpha^R = 0$ (e.g. at the maximum of the $\sigma^R(\alpha)$ curve along the line $\alpha^I = const.$) then it represents the disturbance amplification rate observed in a frame moving with speed $V = -\partial\sigma^I/\partial\alpha^R$. As wavenumber changes from α_m to α_s, V varies from the disturbance group speed c_g to 0 and the amplification rate γ^R changes from maximum to the so-called absolute (observed in a stationary frame). Consequently, choosing the eigenvalue corresponding to the largest value of γ^R enables tracking an asymptotically dominant eigenmode in frames moving with speeds approaching zero.

The above procedure was inspired by the work of Deissler [20] and appears topographically similar to what sometimes is referred to as the continuation technique. The essence of this technique is described, for example, in [31,41] and is interpreted in the context of this paper as follows. The maximum of σ^R is systematically searched along a set of lines $\alpha_k^I = k\Delta\alpha^I$, $k = 0, 1, 2, \ldots$ in the complex wavenumber plane for some small value of $\Delta\alpha^I$. This is the most expensive part of this continuation procedure because a sufficiently large number of eigenvalue problems has to be solved for each fixed value of α_k^I with different α^R to find the location of the σ^R maximum and its value. The step number k increases until the maximum value of σ^R becomes negative. The translational velocity $V = -\partial\sigma^I/\partial\alpha^R$ is computed at the σ^R maximum for each k. Then this continuation procedure is repeated for the negative values of k [26, e.g.]. In this way a complete range of frame velocities V is systematically computed for which amplifying disturbances ($\gamma^R > 0$) are observed, see line I in Fig. 9 which will be discussed in more detail later. This is a major finding in such an investigation [31]. If the obtained velocity range includes only velocities of the same sign the instability is convective, otherwise it is absolute. Therefore if the above continuation procedure is used, the conclusion about the spatio-temporal nature of instability, which is the major goal of the current study, arises as a corollary of a more comprehensive analysis rather than as its direct result. This is why using the continuation procedure to locate transition between absolute and convective instabilities in multi-parameter space is numerically expensive. Indeed a reliable implementation of a continuation procedure requires searching the exact location of the σ^R maxima along the sufficiently dense regular grid of the $\alpha_k^I = const.$ lines [26]. Although each of the found maxima provides accurate information about the amplification rate observed in a frame moving with some velocity V (see Fig. 9) only the amplification

rate $\sigma_s^R = \gamma_{V=0}^R$ observed in a stationary frame $V = 0$ is needed to determine the character of instability. Hence, the numerical expense. In contrast to this continuation procedure which is an analytical tool in its own rights (and which will be used as such to justify some of the numerical steps of Section 3.3) the eigenvalue tracking based on γ^R ordering suggested here is a supplementary technique which is used in conjunction with direct iterative search of a saddle point corresponding to $V = 0$ only. Numerical saving is achieved because the iterations effectively bypass all nonzero values of the translational frame velocity since it is not required that the condition $\partial\sigma^R/\partial\alpha^R = 0$ is satisfied exactly during the iterations for all intermediate values of α^I between 0 and α_s^I. It is sufficient that the search follows the hill of the $\sigma^R(\alpha)$ surface from α_m (black triangle in Fig. 3) to α_s (black circle in Fig. 3) only approximately. This happens naturally during the iterations when the eigenvalues are ordered using the corresponding values of γ_j^R. In contrast to a continuation procedure, an iterative search only requires to solve a single eigenvalue problem at each iteratively chosen value of α^I. The irregular solid line in Fig. 3 shows the convergence of an iterative (simplex in this case) saddle point search algorithm. Neither does it coincide with the dotted line in Fig. 3 (or line I in Fig. 8) showing the hill of the $\sigma^R(\alpha)$ surface which would have to be first found and then followed exactly by a standard continuation procedure, nor is $\Delta\alpha^I$ small during the iterations as would be required by the continuation procedure. In fact, the iterative path to a saddle point can even overshoot the saddle point significantly before finally converging to it. Yet this does not result in a significant increase of computational time as would happen if an overshoot occured in a standard continuation approach. Finally, note that the implementation of a regular continuation procedure which requires locating the hill of the $\sigma^R(\alpha)$ surface as a maximum of the $\sigma^R(\alpha)$ along the lines parallel to the real α axis is likely to fail unless a reliable eigenvalue tracking is implemented. Indeed while the required hill is topographically prominent near the real α axis, deeper in the complex plane it may be covered by other Riemann sheets (eigenvalue surfaces) which have nothing to do with the temporal branch of NDR defining the type of instability, see Fig. 1 (c). On the other hand, even though Fig. 1 (c) shows that the temporal branch of NDR which forms a hill (and a saddle point) is covered five times, still it is easy to identify in plot (e) as there it corresponds to the largest value of parameter γ^R (the line marked by triangles in the vicinity of α_s) over a wide range of wavenumbers. Therefore the required Riemann sheet of NDR is reliably tracked up to the saddle point using the suggested eigenvalue sorting procedure. Note also that in the depicted case $\gamma^R(\alpha_s) = \gamma_{V=0}^R = 0$, i.e. the considered regime may correspond to transition between absolute and convective instabilities.

Consequently, evaluation of γ_j^R at every point along the path of the iterative saddle point search resolves two important problems simultaneously: it tracks the required branch (Riemann sheet) of a fully numerical dispersion relation using only local information, and it determines the character of instability

when evaluated at a saddle point. Also note that the evaluation of γ_j^R does not involve any extra cost as the required derivatives are already computed when the saddle point condition (1) or (5) is evaluated.

While the advantages of the γ^R-based eigenvalue sorting are shown above this technique might also encounter difficulties. Note irregularities in Fig. 1 (e). The γ^R-sorting reliably identifies required eigenvalues over a wide range of wavenumbers but fails at several isolated σ^R-collision points. There are two reasons for this. Firstly, the finite difference formulae of eigenvalue derivatives used to evaluate γ_j^R may jump from one branch to another when evaluation of γ^R is attempted in the $\Delta\alpha$-neighborhood of a collision point. This invalidates the finite difference approximation of derivatives but the problem can be easily fixed by decreasing $\Delta\alpha$ used in the finite difference formulae. Secondly, the "collision" points may correspond to eigenvalues of higher multiplicity (temporal branch points). Standard eigenvalue solvers may lose their accuracy in such a situation. Then inaccuracy of numerically obtained eigenvalues is amplified even more when they are used to approximate derivatives [26]. Therefore it is possible that in the due course of an iterative saddle point search some computed values of γ_j^R will be corrupted invalidating the required eigenvalue ordering. However in contrast to other eigenvalue tracking techniques discussed above this can only happen at isolated points in the complex wavenumber space and usually away from the hill of the $\sigma^R(\alpha)$ surface as illustrated by Figs 1 (c) and (e). Therefore the failure of the γ^R sorting although possible is significantly less likely and damaging than that of other eigenvalue sorting techniques. Yet numerical experiments show that encountering even a single isolated numerical singularity of this sort can throw a saddle point search such as Newton or even Powell [39] iterations completely off course. Yet a simplex method was found to be quite insensitive to such isolated singularities and converged in all computations performed by the author without any human intervention. The only evidence of the fact that simplex iterations did encounter isolated singular points where the eigenvalue tracking failed and functional (5) was evaluated incorrectly was a larger than usual iterative wavenumber increment resulting in an overshoot beyond the saddle point, see Fig. 3. However, since the eigenvalue tracking procedure based on the γ^R sorting remains valid beyond the saddle point this overshoot did not result in the ultimate search failure but just slowed it down by a few iterations. This explains why the use of a relatively slow simplex algorithm which does not require evaluation of higher derivatives may be a safer option in comparison with a generally faster converging Newton method at the initial stage of a saddle point search: large errors in approximating Jacobian in the vicinity of "collision" points cause Newton method to diverge, while a method based on function evaluation is influenced by irregularities to a much smaller degree. Once a simplex (or any other derivative-free) method is used first to minimize (5) to a sufficiently small level, the likelihood of further eigenvalue collisions and irregularities is reduced and then Newton iterations can be safely used to

locate a saddle point accurately and efficiently.

For the sake of completeness we note that in a relatively rare situation when the isolated singularity associated with the σ^R collision is encountered in close vicinity of a saddle point the above procedure may not perform well even if the simplex method is used throughout the iterative search. Such a situation was found in the analysis of atmospheric front instabilities and described to the author by Dr D.G. Duffy [40]. The full convergence could not be achieved because the iterative path kept returning towards the saddle point just to be pushed away from it by the nearby numerical singularity. Such a problem can be fixed by implementing a two-way eigenvalue sorting procedure similar to that discussed in the beginning of this section but combining γ^R and σ^I sorting.

The definition of $\gamma^R = \sigma^R - \alpha^I V$ can be used to determine whether the required saddle point is in the upper or lower half of the α plane. Since the positive maximum of σ^R evaluated at real α is the maximum possible temporal amplification rate observed in a coordinate system moving with the group speed, the value of σ^R must decrease towards the saddle point because the absolute growth rate $\sigma^R(\alpha_s)$ is the amplification rate observed at a stationary system and therefore $\sigma^R(\alpha_s) \leq \sigma^R(\alpha_m)$. It follows from the Cauchy-Riemann conditions that $V = c_g = -\partial\sigma^I/\partial\alpha^R = \partial\sigma^R/\partial\alpha^I$ along the real α line. Then in order to guarantee the decrease of σ^R towards the saddle point one must move down from the real axis if $c_g > 0$ and up if $c_g < 0$. This conclusion is consistent with that of [20] where it was formulated as an observation without proof. It can be straightforwardly used to resolve the eigenvalue identification problem illustrated in Fig. 2. The slopes of the σ^I lines indicate that the group speed is positive (negative) for the wave packet whose characteristics are shown by the line marked by the "+" signs (plain solid line). Therefore the eigenvalue marked by the "+" symbols will form a saddle point in the lower half of the complex α plane and should be tracked for $\alpha^I < 0$. This follows automatically from the bottom right plot in Fig. 2: the eigenvalue marked by the plus signs corresponds to the larger value of parameter γ^R and thus has to be followed for $\alpha^I < 0$.

The saddle point search procedure based on temporal instability analysis which involves computing $\sigma(\alpha)$ branches of NDR was described in this section. This procedure is designed to automatically overcome two major technical difficulties associated with the presence of multiple branches of NDR: tracking the required Riemann sheet and stabilization of the iterative search procedure. These difficulties are not specific to the temporal instability approach. The issue of distinguishing multiple branches arising in a spatial instability-based approach [16,21] is equally severe. Since the spatial instability approach is numerically more complicated due to its nonlinearity the possibility of its automatization is less likely. Therefore solving NDR for $\sigma(\alpha)$ seems preferable.

Although the numerical procedure described in Section 3.1 resolves the major problem with automatization of a saddle point search, locating the saddle point of NDR and checking the sign of the absolute growth rate is not sufficient to make a final conclusion about the character of instability. It has to be shown that the found saddle point is relevant i.e. it is a genuine pinch point of the dispersion relation. Such a point is formed by two spatial branches $\alpha(\sigma)$ of NDR originating in the upper and lower halves of the complex α-plane when σ^R is fixed to a sufficiently large value [3] (see the saddle point marked by black circle in Fig. 3). If such pinching condition is not satisfied (e.g. the saddle point marked by an empty circle in Fig. 3) the asymptotic contribution of this saddle point does not result in absolute instability even if $\sigma^R(\alpha_s) > 0$, see [5,6,8].

Checking the pinching condition is a very expensive computational exercise. Constructing spatial branches requires either solving nonlinear eigenvalue problem as discussed in Section 2 or computing the complete global network of $\sigma^R = const.$ contours over the complex wavenumber plane. The former would annihilate any computational advantages achieved by applying the procedure of Section 3.1 and therefore the latter is commonly used. Unfortunately, the global topography is strongly problem-dependent so that in practice even if it is constructed its visual inspection is required on a case-by-case basis. To demonstrate these difficulties refer Fig. 3 which corresponds to the saddle point discussed in Section 3.1. In order to construct it, 900 temporal eigenvalue problems (2) were solved on a 30×30 grid in the complex wavenumber plane over a region containing both the real α axis and the saddle point. Another 900 eigenvalue problems were solved on the same wavenumber grid with slightly changed discretization of the governing equations so that the spurious eigenvalues could be filtered out. Then ten leading eigenvalues σ_j which were sorted in the descending order of their real parts by a numerical solver were stored at each point. This array of 9000 eigenvalues was still not suitable for creating Fig. 3 because of the irrelevant ordering of the eigenvalues at each point. Reordering them over the complete wavenumber range using parameter γ^R required solving another 900 eigenvalue problems on a slightly shifted grid in the α plane to allow for the finite difference approximation of derivatives

[3] This is true if the considered disturbance wavenumber range includes all wavenumbers with $-\infty < \alpha^R < \infty$. In some problems it is convenient to take into account the symmetry of the wavenumber/frequency spectrum and consider only $0 \leq \alpha^R < \infty$. The treatment of a pinching condition in this case could formally be different from that given by Briggs [7]. The corresponding discussion can be found in [32]. Considering only the positive range of wavenumbers may not be sufficient for checking the pinching condition if the saddle point is found at the imaginary α axis as in example of Fig. 5 considered by Kupfer et al [4].

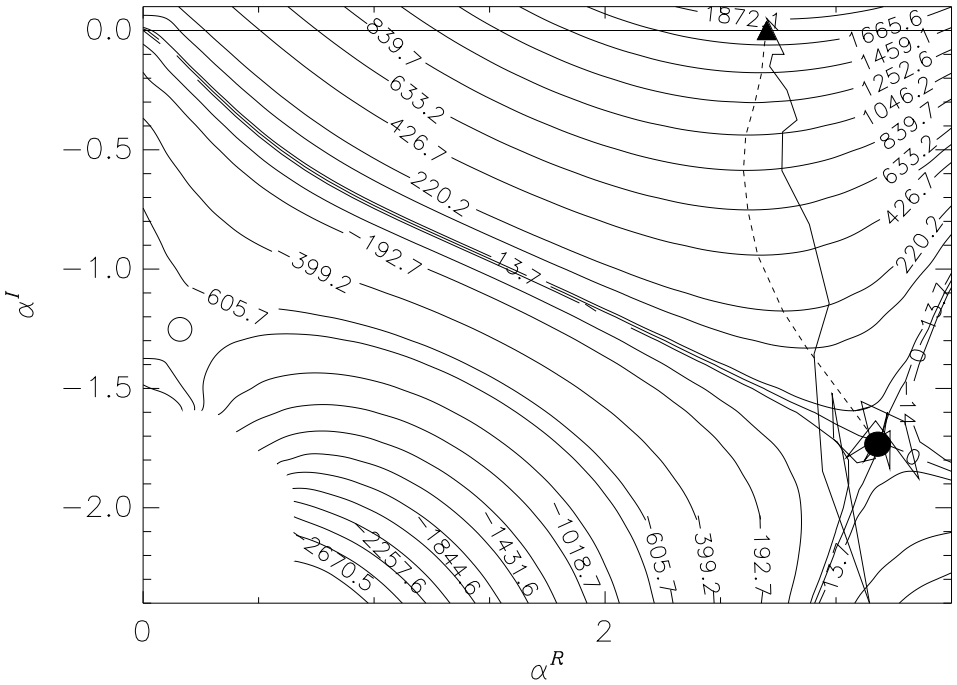

Fig. 3. Level curves of the $\sigma^R(\alpha)$ surface for $(Re, Gr, \epsilon) = (2000, 407705, 0.005)$. The dotted line follows the hill of the $\sigma^R(\alpha)$ surface, the irregular solid line shows the (simplex) iteration path from α_m (black triangle) to a pinch saddle point (black circle). The empty circle shows the location of a saddle point which is not a pinch point. The horizontal solid line corresponds to the original undeformed contour $\alpha^I = 0$.

entering parameter γ^R, but it still was not fully successful. Indeed, by construction, the largest value of γ_j^R is guaranteed to identify the required Riemann sheet only near the top of the hill of the σ^R surface connecting α_m and α_s. As seen from Fig. 1 (e) for wavenumbers α which are sufficiently far to the right from α_s the largest parameter γ^R does not identify the required branch of NDR anymore. Thus while of great help in locating a saddle point, computing γ^R does not resolve all difficulties in constructing the global topography.

Great numerical cost and the necessity of a visual inspection of the global topography makes checking the pinching condition at every point in a multi-parameter space impractical when a complete CAIB involving thousands of points has to be determined. For this reason the check is normally done only for selected points and then it is assumed that the qualitative topography of $\sigma_j(\alpha)$ does not change in between the tested points [12,37,27]. Obviously, the more complicated the physical problem is, the more nonlinear NDR becomes, the more difficult it is to construct a global picture for a reasonable number of test points. The danger of missing a qualitative change in topography and making a wrong conclusion about the spatio-temporal character of instability increases. Therefore an alternative, computationally more efficient local check of pinching condition is needed. It can be done using the approach of [4]. There

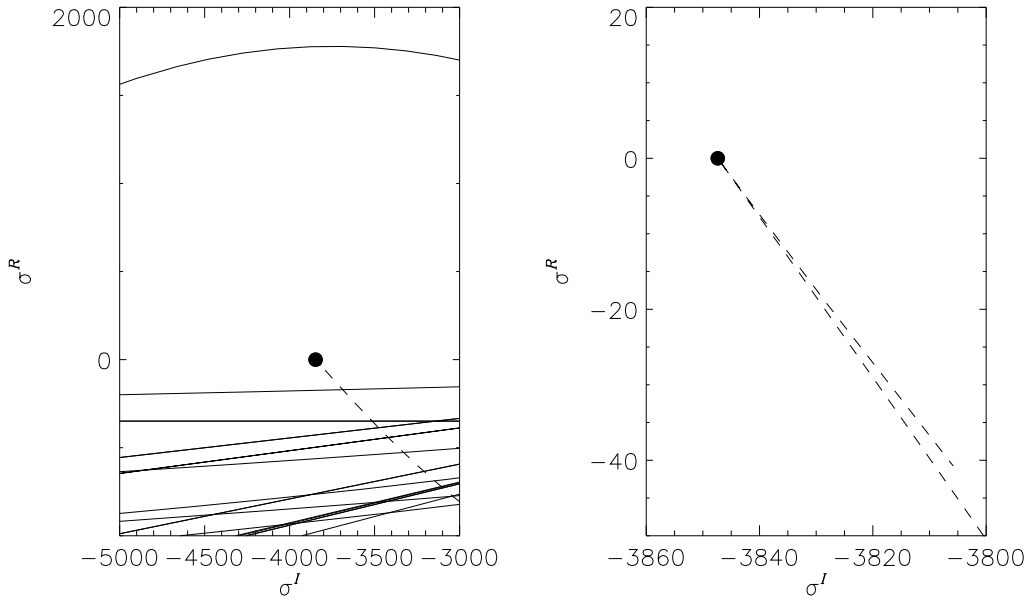

Fig. 4. Cusp map for $(Re, Gr, \epsilon) = (2000, 407705, 0.005)$ (left) and its close up (right). The solid and dashed lines show the images of the branches of NDR for $\alpha^I = 0$ and $\alpha^I = \alpha_s^I$, respectively. The cusp point is shown by a circle.

the authors showed that the path $\alpha^I = \alpha_s^I$ through a saddle point of the $\sigma^R(\alpha)$ surface is mapped into a path forming a cusp in the complex σ plane. As was discussed in Section 2 locating a cusp point normally would require a visual inspection and, consequently, could not be done automatically [27]. On the other hand, once the saddle point is accurately determined via the automatic procedure described in Section 3.1 the cusp point $\sigma = \sigma(\alpha_s)$ is known as well. According to the proof given in [4] the check of the pinching condition then is reduced to counting how many times the cusp point is covered by the the temporal branches of NDR computed along the real α axis. Most importantly, this does not require *any* extra computations as all required temporal branches have already been computed at the very first step of the saddle point search procedure of Section 3.1. The procedure replacing the construction of a global picture of Fig. 3 is illustrated in Fig. 4 where the images of σ along the paths $\alpha^I = 0$ and $\alpha^I = \alpha_s^I$ are presented. The cusp point (circle) is covered from the top only once (odd number of times) by images of the temporal branches (solid lines) which means that it is a genuine pinch point according to [4]. Note that solid lines in Fig. 4 are images of branches of NDR shown in the top plot in Fig. 1. They may remain sorted according to the size of their real parts as in temporal stability analysis because only the knowledge of σ_j^R is required in this approach to conclude whether the pinching condition is satisfied. In practice construction of Fig. 4 and its visual inspection are not necessary. Indeed once the characteristics of a saddle (cusp) point are established one only needs to count how many temporal eigenvalues (which have already been

computed for $\alpha^I = 0$) whose imaginary parts $\sigma_j^I = \sigma_s^I$ have the real part which is larger than σ_s^R. This can be done automatically as the information about all eigenvalues for real α is known from the start. Finally, note that the cusp-forming curve in the σ plane is typically very sharp as seen from the left plot in Fig. 4. For this reason searching the cusp directly would require very detailed visual inspection of a strongly magnified map as that shown in the right plot of Fig. 4 [27]. This is an impractical and subjective procedure and the iterative saddle point search described in Section 3.1 remains a much more accurate, convenient and efficient alternative.

3.3 Multiple σ^R maxima and multiple saddle points

So far it was implicitly assumed that the $\sigma^R(\alpha)$ curve at real α has a single maximum as in the top plot in Fig. 1 and the required Riemann sheet of the dispersion relation contains only one saddle point which contributes to spatio-temporal instability. However as was pointed out almost four decades ago in [38] neither of these conditions have to always be satisfied in physical problems. This was demonstrated in the author's earlier studies of non-Boussinesq convection [42]. Multiple maxima of the $\sigma^R(\alpha)$ were also found in a rotating-disk boundary layer [8] while multiple saddle points (albeit discussed in the context of the continuation procedure summarized in Section 3.1) were found in the flow along an inclined plane [31], and recently in three-dimensional boundary layers [26] and in Kelvin-Helmholtz instability [32]. It is also worthwhile noticing that multiple maxima of the $\sigma^R(\alpha)$ curve for real α can lead to looping and self-intersection of the image of the real wavenumber axis in the complex σ plane, see the right end of the upper solid curve on Fig. 6. If such a loop encloses a branch (saddle) point the situation would be identical to that of the artificial example presented by Kupfer et al. [4] in their Fig. 5. However the author did not find such a situation neither in his own computations nor among the physical results reported by other authors so far and thus it is not discussed here in detail.

In the author's studies, added physical nonlinearities associated with fluid property variations with temperature in non-Boussinesq mixed convection lead to the situation illustrated in Figs 5–7 which exists in a wide range of physical parameters. The top plot in Fig. 5 shows that the leading branch of NDR has two distinct maxima located at α_{m1} and α_{m2}, $\alpha_{m1} < \alpha_{m2}$. These maxima can be traced back to different terms in the governing equations and therefore they represent physically different mechanisms of instability. Linearly, these two maxima can be viewed as representing two disturbance wave envelopes propagating each with its own group speed and characterized by its own dominant wavenumber α_{m1} or α_{m2}. The edges of these envelopes can overlap and therefore the distinction between them might be hard to establish experimen-

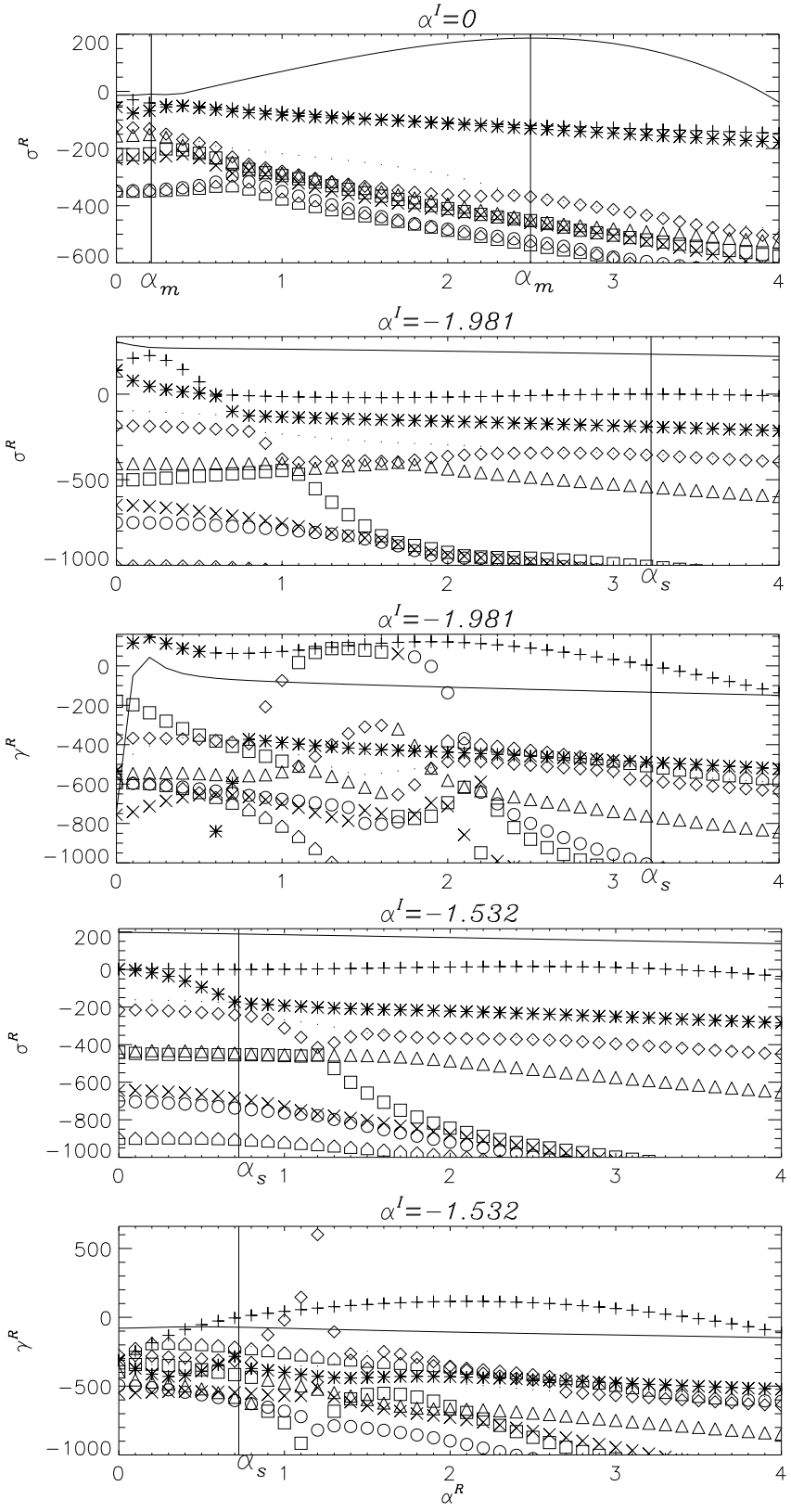

Fig. 5. Temporal branches of NDR and parameter γ^R in the complex wavenumber plane for $(Re, Gr, \epsilon) = (239, 49898, 0.3)$. Different symbols are used to distinguish between eigenvalues sorted by a numerical code in the descending order of σ^R.

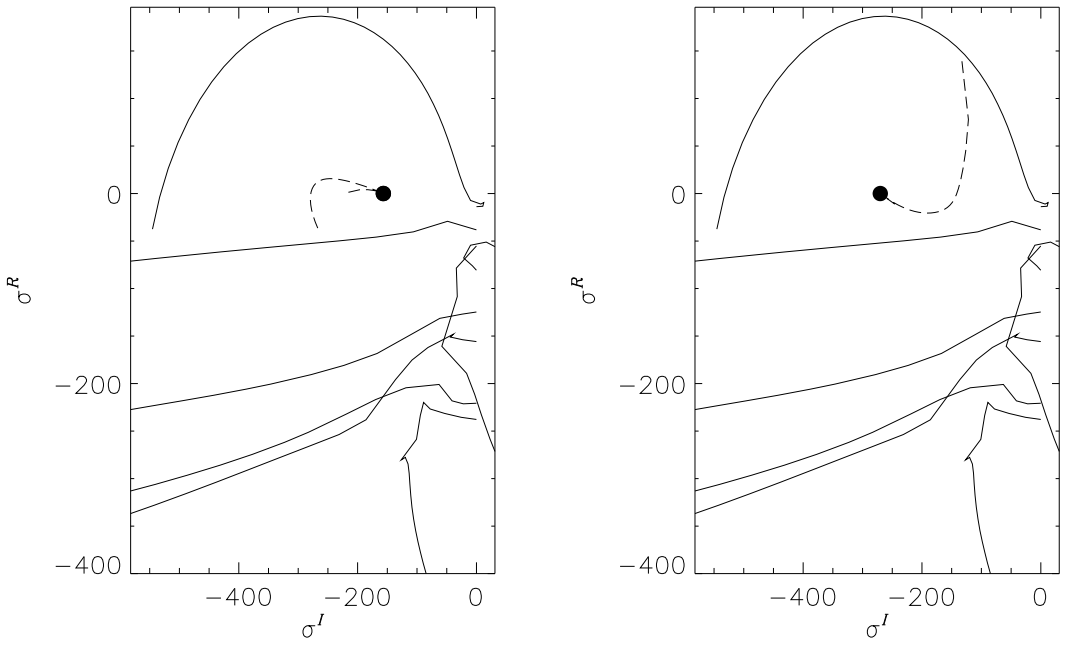

Fig. 6. Cusp maps for $(Re, Gr, \epsilon) = (239, 49898, 0.3)$: the left and right plots correspond to the left and right saddle point in Fig. 7, respectively. The solid and dashed lines show the images of the branches of NDR for $\alpha^I = 0$ and $\alpha^I = \alpha_s^I$. The cusp points are denoted by circles.

tally. However if at least one of these envelopes is absolutely unstable then the flow is guaranteed to be absolutely unstable. Therefore following the procedure described in Sections 3.1 and 3.2 we look for CAIB by initiating the iterative saddle point search first at α_{m1} and then at α_{m2}. In this way, two distinct saddle points are found at α_{s1} and α_{s2}, which happened to be in the top left (just above the real α axis) and in the bottom right corners of Fig. 7, respectively. Although the possibility of the existence of multiple maxima was first noted several decades ago (e.g. [38] and references therein) the validity of the above approach does not appear to be discussed with sufficient theoretical rigor to date. However the success of the saddle point search using the outlined procedure is not accidental. It can be foreseen based on the continuation procedure outlined in Section 3.1, even though such a procedure is not used in practical computations here. Indeed as discussed for example in [31] the maximum of the $\sigma^R(\alpha)$ curve for real α corresponds to the saddle point of a dispersion relation written for a system moving with the group speed of a wave envelope centered at the wavenumber corresponding to this maximum. Small variation of the frame speed leads to continuous displacement of the saddle point into the complex wavenumber plane (reference [31] proves this using the Taylor series expansion of a dispersion relation). These arguments can be extended to the situation where several maxima exist and therefore it can be concluded that the saddle point corresponding to each of the maxima exists for some range of frame velocities [8]. Since our goal here is detecting the transition to absolute instability this range should include zero velocity.

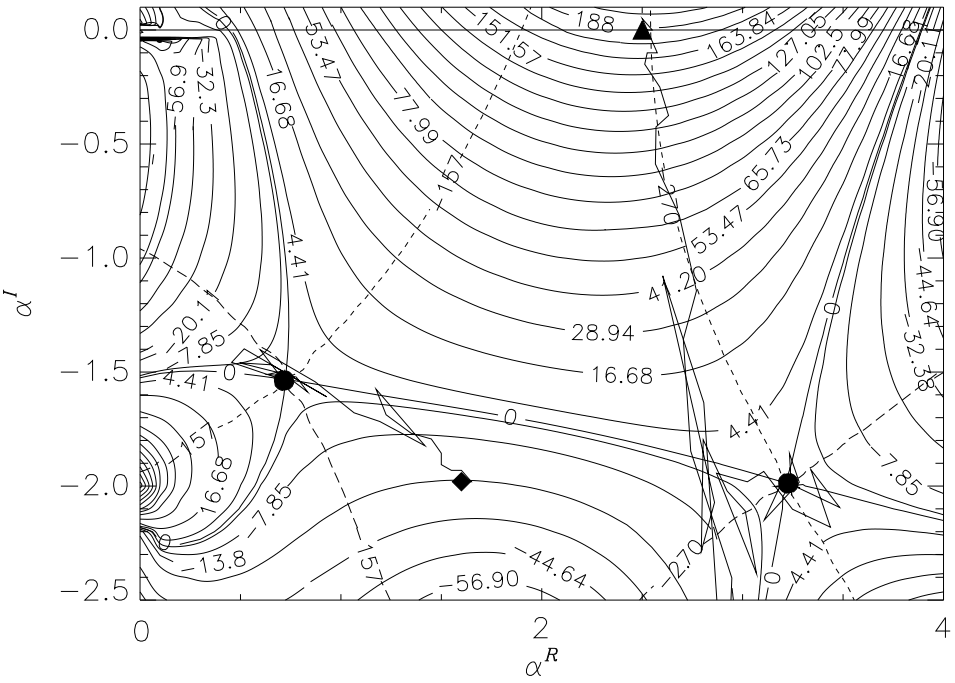

Fig. 7. Level curves of the σ^R surface for $(Re, Gr, \epsilon) = (239, 49898, 0.3)$. The dotted and dashed lines are the level curves of the $\sigma^I(\alpha)$ surface passing through the saddle points (black circles) which show the steepest descent paths to and from the saddle points, respectively. The horizontal solid line corresponds to $\alpha^I = 0$, the irregular solid lines originating at black triangle and black diamond show the iterative saddle point search paths.

However no proof is yet readily available that this is indeed always the case when multiple maxima are present. Therefore in practice it is suggested to always initiate the iterative saddle point search from each of the maxima α_{mi}, $i = 1, 2, \ldots$. If such a search converges and a saddle point (1) corresponding to $V = 0$ is found then the sign of $\sigma^R(\alpha_{si})$ is determined and, if it is positive, the pinching condition is checked to confirm the absolute nature of instability associated with the wave envelope centered at α_{mi}. Divergence of the iterative saddle search would signal a singular situation caused by non-analyticity of a dispersion relation. Such situations would require a more comprehensive analysis. However so far they were not encountered in the author's own computations nor were they reported in any of the studies known to the author.

Since it is found that $\sigma^R(\alpha_{s1}) < 0$, checking the pinching condition for this point is not required as even if it is a genuine pinch point it cannot lead to absolute instability because the corresponding wave envelope has negative growth rate in a stationary frame. On the other hand the second saddle point has $\sigma^R(\alpha_{s2}) = 0$ and is a clear candidate for determining transition to absolute instability. This saddle point is located relatively far away from the real α axis (at $\alpha^I = 1.981$) and the value of $\sigma^R(\alpha_{s2})$ is not the largest (it is the second largest, see the line marked by the "+" symbols in the second from the top

plot in Fig. 5). Therefore the automatic iterative search of this saddle point becomes possible only upon using some eigenvalue tracking algorithm such as that of Section 3.1: the corresponding value of γ^R remains the largest even though the iterative path shown by the irregular solid line in Fig. 7 is far from that required by a standard continuation procedure outlined in Section 3.1. The automatic check of a pinching condition discussed in Section 3.2 is also successful and confirms that this point is relevant (see the right plot in Fig. 6 which also illustrates this fact). Since the value of $\sigma^R(\alpha_s) = 0$, the considered regime seems to correspond to a point on CAIB. However a more careful consideration shows that this is not so. It turns out that the considered Riemann sheet contains another saddle point at α_{s3}. It is clearly seen in the left part of Fig. 7. In contrast to the left saddle point seen in Fig. 3 it satisfies the pinching condition (see the left plot in Fig. 6) [4] and it happens to lie on slightly higher grounds with respect to the first saddle point. This means that the conclusion that the transition to absolute instability was just detected is wrong, the flow is already absolutely unstable owing to the contribution of a second saddle point. Yet as seen from Fig. 7 the saddle point search initiated at α_{m2} (black triangle) whose iterative path (irregular solid line originating from a black triangle) essentially follows the steepest descent path towards the right saddle point (dash-dotted line) and fails to detect it. A similar failure of the standard continuation procedure which follows the maximum of the $\sigma^R(\alpha)$ surface was reported in [31,26,32] and its reason was stated as a saddle point bifurcation. In the context of this work we note that the second saddle point is caused by the existence of the second hill of the $\sigma^R(\alpha)$ surface such as the one seen in the left half of Fig. 8 which is not connected to that at α_{mi} by continuity. This second hill is seen as an additional maximum in Fig. 5 separated from the first one by a minimum when α^I is fixed to some nonzero value, see the lines marked by the "+" symbols in the second and fourth from the top plots. As noted in [31] and will be discussed below, the additional saddle point is due to the fact that the problem's dispersion relation is multi-valued at some complex values of α (the presence of "true" eigenvalue collisions i.e. eigenvalues of multiplicity two).

It is an alarming fact that the search algorithm of Section 3.1 did not locate the dominant saddle point α_{s3}. Part of the problem is that the numerical results obtained for real α give no hint on whether additional significant saddle points not directly related to the maxima of the $\sigma^R(\alpha)$ curve at real α exist somewhere in the complex wavenumber plane. It is also stated in [31] that the

[4] Comparison of Fig. 3 and Fig. 7 shows that we are dealing with the so-called pinch dissolution due to the interaction of two neighboring saddle points: the situation when the saddle points undergo a qualitative change from pinching to non-pinching and vise versa as the physical parameters change. This was first discussed in [38] in the context of plasma physics but appears to be a relatively common situation in fluid mechanics studies.

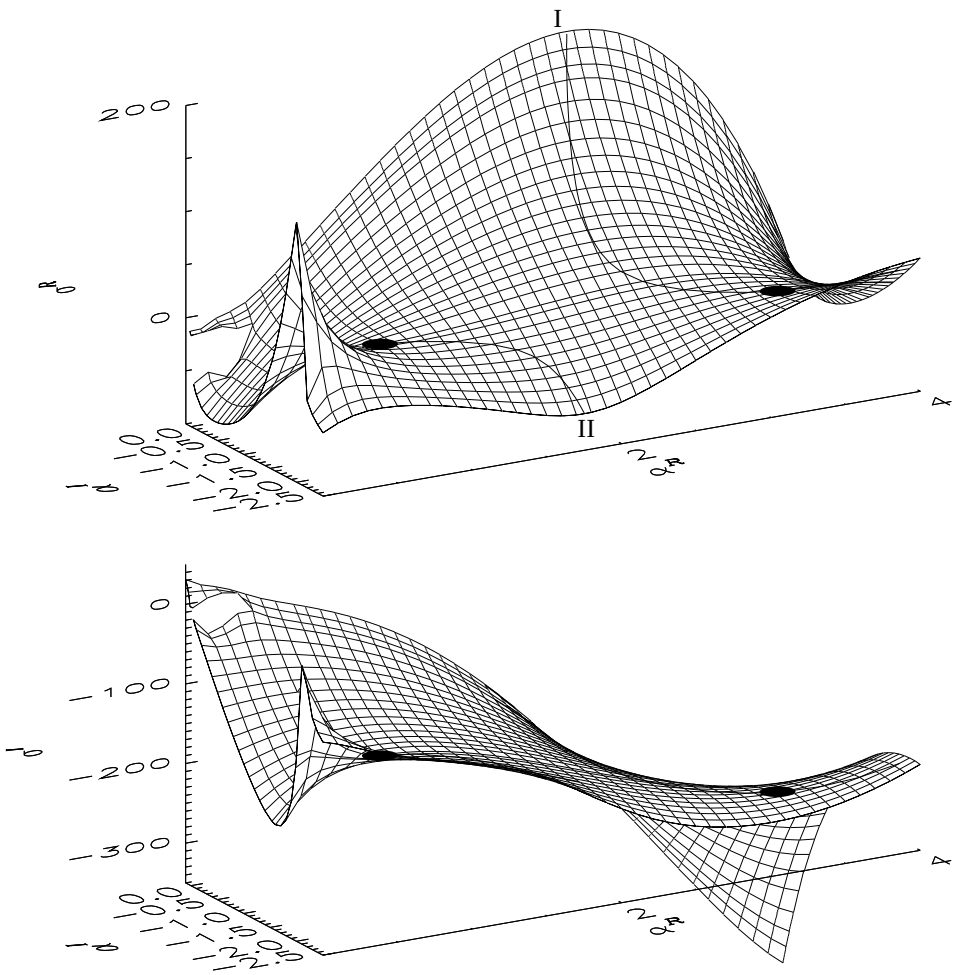

Fig. 8. The surfaces $\sigma^R(\alpha)$ (top) and $\sigma^I(\alpha)$ (bottom) representing the Riemann sheet containing the dominant saddle points (shown by black disks) of a dispersion relation for $(Re, Gr, \epsilon) = (239, 49898, 0.3)$. Lines I and II follow the maximum and minimum of the $\sigma^R(\alpha)$ surface when cut by the $\alpha^I = const$ planes.

orientation of the steepest descent path from a saddle point contains no direct information concerning the existence of an equivalent steepest descent path and therefore of a second saddle point. For this reason in [31] spatial roots of the dispersion relation were found and their collisions were visually analyzed to detect spatio-temporal characteristics of instability. This is computationally less efficient than finding the temporal roots of the dispersion relation. Fortunately the situation with finding the saddle points formed by temporal branches of NDR is not as hopeless as it appears at first sight. The following topological arguments suggest how the presence of additional saddle points can be indicated without opting for a greatly more expensive computations of spatial roots.

Assume that the saddle point search procedure suggested in this paper and initiated at α_{m2} resulted in a saddle point α_{s2} at which $\sigma^R(\alpha_{s2}) = 0$ and which is a genuine pinch point, see Fig. 7. Clearly, it is a candidate to define the

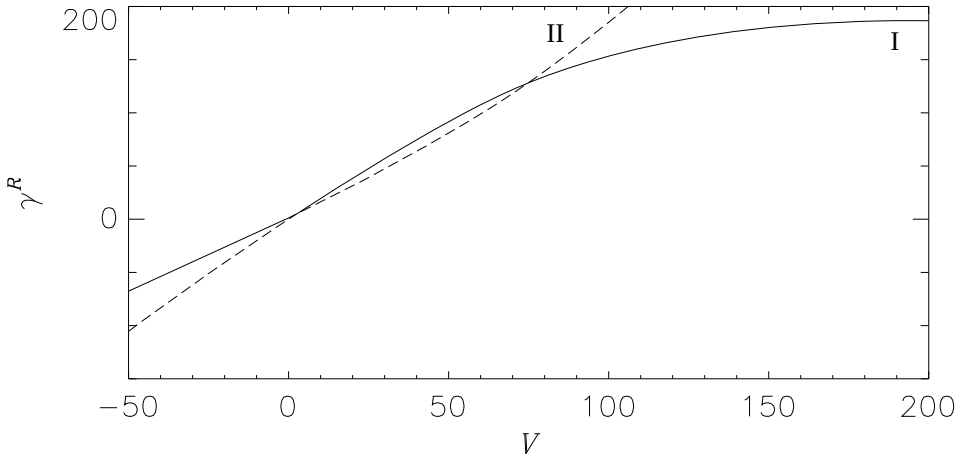

Fig. 9. The real amplification rate γ^R observed in a frame moving with velocity V for $(Re, Gr, \epsilon) = (239, 49898, 0.3)$. Lines I and II correspond to the branches obtained by continuation along the hill and the valley of the $\sigma^R(\alpha)$ surface. Segments of the branches formally obtained from non-pinching saddle points are shown by dashed lines.

transition to absolute instability. However this is only so if there are no other saddle points satisfying the pinching condition which are located at higher grounds with respect to $\sigma^R(\alpha_{s2})$. By construction $\sigma^R(\alpha_{s2})$ belongs to the hill of the $\sigma^R(\alpha)$ surface and therefore it must be located at the "nose" of the U-shaped $\sigma^R = const.$ contour protruding into the complex wavenumber plane from the real α axis as seen in Fig. 7. The specific U-shaped form of contours is enforced by the fact that $\sigma^R(\alpha)$ has a maximum along the real α axis so that $\sigma^R = const.$ contours connect the points with equal amplification rate located on the either side of this maximum. Since at a saddle point $\frac{\partial \sigma^R}{\partial \alpha^R} = 0$, the contour forming it has a tangent parallel to the real α axis as it approaches the saddle point. Therefore this saddle point is necessarily located at the maximum possible distance from the real α axis along the U-shaped $\sigma^R = 0$ contour. If another saddle point α_{s3} exists which is not related to the hill originating at α_{m2}, it can only be asymptotically significant if it, like α_{s2}, is formed by the U-shaped contours. This is so because these are the only contours which retract completely to the other half of the complex α plane when σ^R increases as required by the pinching condition [6, e.g.], see Fig. 7. In addition, in order to contribute to absolute instability this saddle point must have $\sigma^R > 0$. This means that it should be located uphill from α_{s2}, i.e. closer to the real α axis so that $\left|\alpha^I_{s2}\right| > \left|\alpha^I_{s3}\right|$, and the U-shaped contours should approach it from the $\alpha^I = 0$ and/or from the $\alpha = \alpha_{m2}$ lines. On the other hand, the counterparts of the U-shaped contours forming such a saddle point and corresponding to the increasing σ^R levels must remain in the same half-plane as α_{s2}. This is only possible if a second hill distinct from that containing α_{s2} exists in the same half-plane. Moreover, since the U-shaped contours corresponding to the increasing σ^R levels move towards the real α axis and towards α_{m2} their counterparts must move generally in the opposite

direction, i.e. towards the line $\alpha^I = \alpha^I_{s2}$, but away from the line $\alpha^R = \alpha^R_{s2}$. This means that the second hill of the $\sigma^R(\alpha)$ surface, if exists and leads to a saddle point α_{s3} satisfying the pinching condition, should be separated from the first hill containing α_{s2} by the valley which indeed is seen in the top plot in Fig. 8. As follows from the above discusion the second hill should continue away from the real α axis. Then the presence of the valley separating the two hills may be detected by inspecting the $\sigma^R(\alpha)$ curve obtained along the straight line $\alpha^I = const.$ issued from the saddle point at α_{s2}: if the second hill exists then this curve will have a characteristic minimum, see the line marked by the "*" and "+" symbols in the second top plot in Fig. 5.

Therefore the possible presence of an additional relevant saddle point is strongly indicated by the minimum of the $\sigma^R(\alpha)$ curve computed for $\alpha^I = \alpha^I_{s2}$ (see also [26] for some numerical recipes in this regard for three-dimensional flows). Once such a minimum is detected, finding a second saddle point has to be attempted. The location of this minimum (shown by the diamond symbol in Fig. 7) may be conveniently used as a starting point for an iterative search of the saddle point α_{s3}. This time the iterative search approximately follows the bottom of the valley of the $\sigma^R(\alpha)$ surface. Note that as seen from Fig. 5 the eigenvalue sorting based on γ^R still identifies the required eigenvalues reliably. This is so because at the minimum the condition $\frac{\partial \sigma^R}{\partial \alpha^R} = 0$ is satisfied and therefore parameter γ^R gives the amplification rate observed in a frame moving with velocity $V = \frac{\partial \sigma^I}{\partial \alpha^R}$ which now corresponds to a wave envelope not connected to that centered at α_{m2} by continuity. If this envelope is asymptotically dominant and leads to absolute instability it must have the largest amplification rate, the condition required by the adopted γ^R sorting of eigenvalues. This is indeed the case and is seen in Fig. 9 which is qualitatively identical to Figure 7(a) in [31]. Although the construction of such a diagram is not required to determine transition to absolute instability it is instructive to discuss it and show how the current computational approach relates to that of [31]. This is done next.

If the standard continuation procedure was used starting at α_{m2} it would follow the top of a larger hill in the upper plot of Fig. 8 towards α_{s2} so that $\frac{\partial \sigma^R}{\partial \alpha^R}$ would remain zero. The corresponding trajectory is shown by line I. For each point of this trajectory the frame velocity $V = -\partial \sigma^I / \partial \alpha^R$ and the the amplification rate (6) observed in this system would be computed and then parametrically graphed in Fig. 9. As expected the maximum growth rate is observed in a system moving with the group speed $c_g = V(\alpha_{m2})$ and it decreases towards zero as line I approaches the saddle point α_{s2} where V becomes zero. If line I were continued to the other half of the α plane then the other half of curve I in Fig. 9 would be obtained for larger positive values of V. This has not been done because the other half of the $\gamma^R(V)$ curve is not needed when the conclusion on whether the instability is absolute or convective is made: only the part of the curve closest to $V = 0$ is important for this purpose. A

similar continuation procedure which starts at the bottom of the valley and which follows it along line II in Fig. 8 would result in branch II in Fig. 9 (cf.[26]). Note that although the valley continues beyond the saddle point for $\alpha^I \gtrsim -1.5$ its orientation changes in such a way that the condition $\frac{\partial \sigma^R}{\partial \alpha^R} = 0$ cannot be satisfied anymore and the continuation trajectory II turns back towards the larger negative values of α^I. Now, for negative values of V, it follows the second hill seen in the left lower corner of the top plot in Fig. 8 (this part of line II is not visible in the figure as it is screened by the hill). In the depicted case, line II in Fig. 9 corresponds to a slightly positive growth rate at $V = 0$ and therefore this branch obtained by continuation along the valley, rather than along the hill, of the $\sigma^R(\alpha)$ surface determines the transition to absolute instability. The pinching condition for the corresponding saddle point for $V = 0$ has been already checked as described earlier in this section. However we revisit this aspect once again from a different point of view to shed more light on the role different saddle points play. Fig. 10 shows the four $\gamma^R(\alpha)$ fields which are obtained from Fig. 7 by applying transformation (6) for $V = -10$, 10, 60 and 90. As seen from the resulting patterns the two saddle points exchange their pinching properties: for negative velocities the left saddle point (obtained by continuation along the valley) is significant as it is formed by the spatial roots $\sigma^R = const.$ originating in different halves of the α plane. On the other hand, for positive velocities the right saddle point (obtained by a continuation from the maximum α_{m2}) is significant. This is a case of pinch dissolution which is discussed in [38] and also found in Kelvin-Helmholtz instability [32], rather than a saddle point bifurcation refered to in [31]: two saddle points always co-exist, but exchange their asymptotic role. Note that for $V \gtrsim 75$ saddle point located in the valley (branch II) formally predicts the larger amplification rate than that on a hill (branch I). However this saddle point remains asymptotically insignificant because the corresponding pinching condition is not satisfied, see the bottom right plot in Fig. 10. The segments of the growth rate branches which are obtained from non-pinching saddle points are shown in Fig. 9 by dashed lines.

It follows from the above discussion that searching a saddle point and checking the pinching condition as suggested in this work are capable of producing results qualitatively identical to those reported in [38,8,31] without solving the problem dispersion relation for its spatial roots $\alpha(\sigma)$. This is especially important if the dispersion relation is highly nonlinear in wavenumber so that finding the spatial roots becomes an extremely challenging task. The only extra computational cost is associated with the need to solve an additional set of standard temporal eigenvalue problems along the line $\alpha^I = \alpha^I_{s2}$ and subsequent iterative search of a secondary saddle points if the shape of the obtained $\sigma^R(\alpha)$ curve indicates their existence. This cost is well offset by the increased reliability of the obtained results and is still much smaller than the cost of constructing a global topography as in Fig. 7 which is given here as an illustration rather than an essential part of the search process. Even with

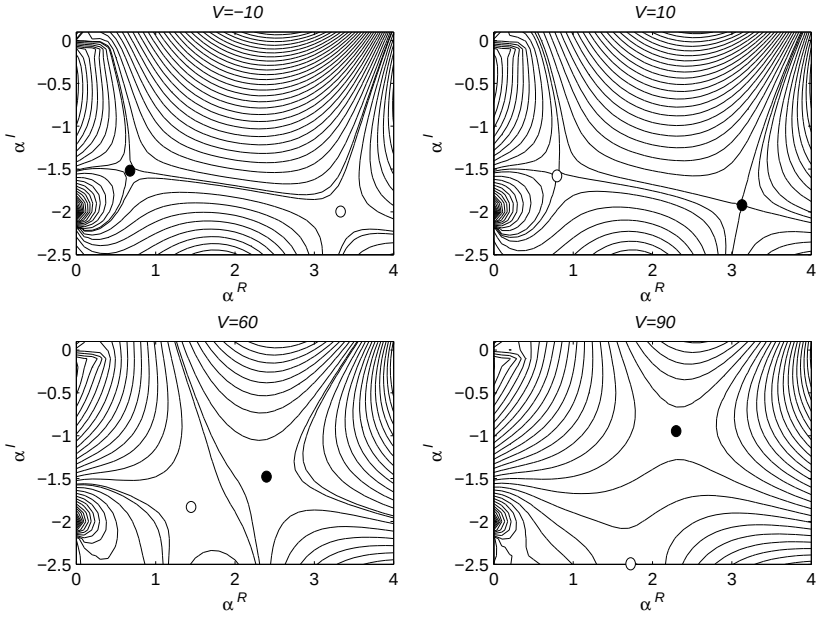

Fig. 10. Pinch dissolution process as the frame velocity V changes for $(Re, Gr, \epsilon) = (239, 49898, 0.3)$. Saddle points satisfying (not satisfying) the pinching condition are shown by solid (empty) circles.

these additional steps the computational procedure described here retains its automatism as finding maxima or minima does not require a visual inspection.

Since the additional computations have to be carried out for a sufficiently wide range of α^R at $\alpha^I = \alpha^I_{s2} \neq 0$ the success of the whole procedure depends crucially on the reliability of the automatic eigenvalue tracking. Numerical experiments showed that the γ^R sorting appears to do a good job even in complicated situations such as those discussed in this section. However note that as seen in the bottom plot in Fig. 5, for numerical reasons discussed in Section 3.1, the γ^R sorting still fails for several isolated points: see the diamond symbols above the "+" symbols. This inevitably leads to an incorrect evaluation of functional (5) and would cause severe problems to most of the minimization algorithms. However as noted earlier, a simplex method copes with such isolated singularities quite well and just requires a few extra iterations (see the loop near the diamond symbol in Fig. 7) to converge: a reliability feature which in many cases outweighs the faster convergence of other algorithms.

In the end of this section we will discuss another important aspect which also sheds light on the multiple saddle point situation. A singularity is clearly seen just below the real α axis in the upper left corner of Fig. 7. It is caused by the "true" collision i.e. by a multi-valued point of the problem dispersion relation which is depicted in Fig. 11. This figure shows that as the value of α^I decreases from 0 to $\alpha^I_b \approx -0.037$ the two eigenvalue branches collide in

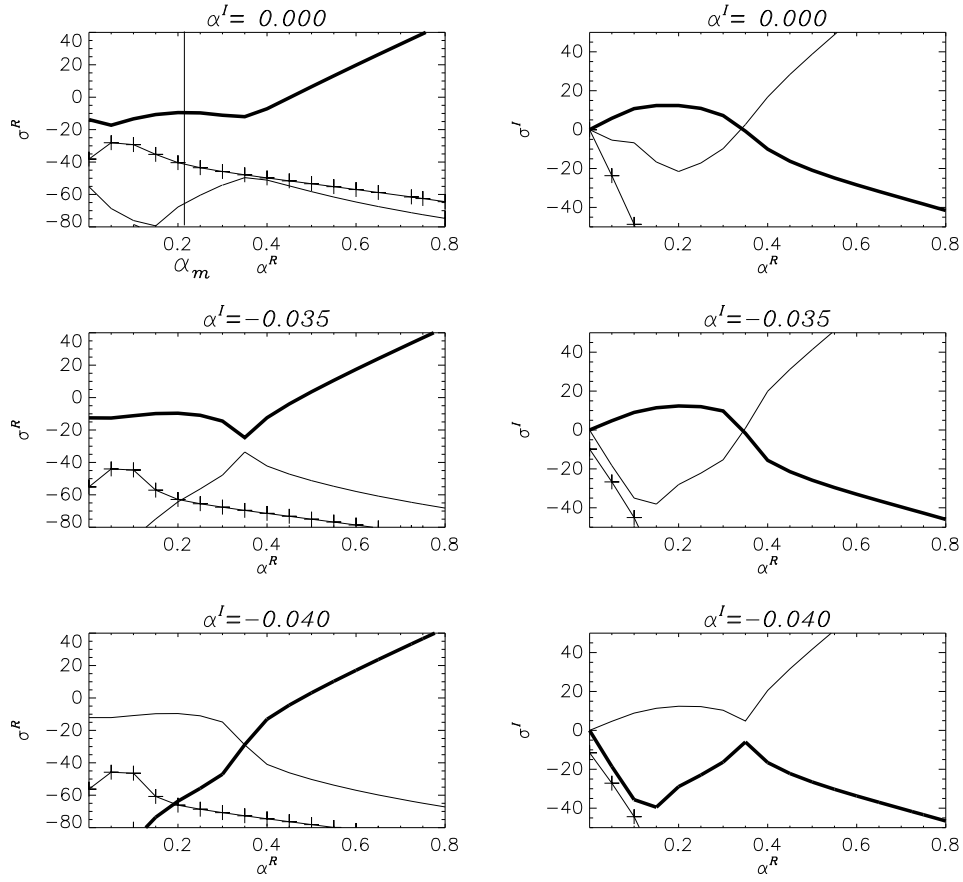

Fig. 11. The $\sigma^R(\alpha)$ and $\sigma^I(\alpha)$ curves in the vicinity of the branch point of the problem dispersion relation seen in the left top corner of Fig. 7. The thick solid lines show the branch of a multi-valued dispersion relation chosen after an appropriate branch cut is introduced.

a "true" way so that the numerical dispersion relation has an eigenvalue of multiplicity two. Note the characteristic cusp forming near the collision point and a cross-over of the $\sigma(\alpha)$ curves. Theoretically continuing the saddle point search beyond α_b^I requires the introduction of a branch cut originating at the collision point, see the top left corner in Fig. 8. This should be done in such a way that the maximum of the $\sigma^R(\alpha)$, $\alpha^I = 0$ attained at α_{m2} belongs to the same branch of NDR as the sought saddle point i.e. the branch shown by the thick solid lines in Fig. 11 should be chosen. The mapping of the corresponding branch cut then appears in Fig. 7 as a very dense cluster of isolines. This is just the way graphing software attempts to represent the jump in σ^R values across the branch cut (see the gap in the top left corner of Fig. 8 and the sudden change in the left sections of thick solid lines in Fig. 11). The presence of such "true" collisions may introduce two theoretical complications best seen from the point of view of the method of steepest descent [8]. Firstly, the required branch cut should be introduced in such a way that it does not prevent the deformation of the original $\alpha^I = 0$ integration contour into the steepest descent path through the saddle points. Secondly, if

$\sigma^R(\alpha_b) > 0$ the branch point itself will contribute to the asymptotic behavior of the system as the deformed contour must go around it so as not to cross the branch cut [5]. Therefore any reliable automatic numerical algorithm for searching CAIB should either have a mechanism to account for the branch point contributions or at least signal their presence. Inspection of Fig. 11 shows that a cusp of the $\sigma^R(\alpha)$ curve exists at a branch point which transforms into a minimum or leads to the intersection of two $\sigma^R(\alpha^R)$ curves in its vicinity. The existence of multiple maxima of the leading $\sigma^R(\alpha)$, $\alpha^I = 0$ curve which are separated by minima then is an indication that the branch points exist in the proximity of the $\alpha^I = 0$ line which should be accounted for. Finding the branch point of NDR in a complex wavenumber space numerically is as challenging as finding a saddle point. Since at a branch point the derivatives forming (5) are infinite one might try to find its location by minimizing the functional reciprocal to (5) i.e. F^{-1} starting at the local minimum of the $\sigma^R(\alpha)$, $\alpha^I = const.$ curve. This is how the accurate location of a branch point was found for Fig. 11. In practice it may be necessary to minimize the functional to a certain finite level only (using the γ^R sorting) and then to finish the search by minimizing the distance $|\sigma_n - \sigma_{n+1}|$ between the two closest eigenvalues in the NDR spectrum, where n corresponds to eigenvalue numbering according to their real parts. The second stage might be necessary to avoid technical difficulties in approximating very large derivatives near the branch point. One also should be aware of possible difficulties experienced by an eigenvalue solver and associated with its handling of eigenvalues of multiplicity two. Finding the branch points of course adds a substantial extra cost to the procedure. In some cases it could be argued that if the values of $\sigma^R(\alpha)$, $\alpha^I = 0$ curve at the minima points are negative then the branch points also have $\sigma^R(\alpha_b) < 0$ so that their asymptotic contributions are negligible and the search of their exact location in the complex wavenumber space is not required. No counter-examples invalidating this assumption were found in the computations performed by the author or known to him from other published studies. However it is not clear at this stage whether this statement is true in general. Therefore finding branch points appears to be a more expensive but safer option. Fortunately, this still can be accomplished automatically. For example, two minima of the $\sigma^R(\alpha)$ curve in Fig. 11 indicate that two branch points exist near the $\alpha^I = 0$ axis. Both of them were successfully found using the discussed procedure. One of these branch points has already been discussed in detail above and the other is found just above the $\alpha^I = 0$ axis. It is formed by colliding thick solid line and the line marked by the "+" signs. However both branch points have $\sigma^R < 0$ and have no asymptotic contribution in this example.

Finally, note that the topological nature of the multiple relevant saddle points as those seen in Fig. 7 emerges in the light of the above discussion. They are signaled by the presence of multiple hills of the $\sigma^R(\alpha)$ surface separated by valleys which indicate the existence of temporal branch points of a multi-

valued dispersion relation. This is the case in Fig. 7: the existence of two saddle points α_{s1} and α_{s2} arising from the two maxima at α_{m1} and α_{m2} are due to the temporal branch point depicted in Fig. 11 while the additional saddle point α_{s3} in the lower half of the α plane is a consequence of a similar temporal branch point, but located at a larger negative value of α^I which is outside the range of Fig. 7.

3.4 Summary of a search procedure

In Sections 3.1–3.3 we discussed in detail major numerical difficulties in searching the transition between the convective and absolute instability regimes most commonly found in spatio-temporal instability studies. The combined procedure described in this paper, although not completely free from limitations discussed in previous sections, suggests how to resolve them in a numerically more efficient and automatic way than could be done by the previously known individual techniques on which it is based. Its major steps are summarized below for convenience.

(a) The linearized disturbance equations are discretised and written in the form of a temporal instability problem which results in a standard linear generalized matrix eigenvalue problem (2) for the complex temporal amplification rate σ.
(b) The physical governing parameters are fixed at some values and the leading eigenvalues are computed using a standard (say, QZ) algorithm and stored for a sufficiently large range of real wavenumbers including all values of α for which $\sigma_j^R(\alpha) > 0$.
(c) Wavenumbers corresponding to all positive maxima and all minima of real amplification rate curves are identified and stored.
(d) The iterative saddle point search is repeatedly initiated at each of the maxima identified at step (c). The search can use the Newton-type iterations driving the value of finite difference approximation of a complex expression $\frac{\partial\sigma}{\partial\alpha}$ to zero. If the convergence cannot be achieved then initial iterations should be attempted using a method not requiring numerical Jacobian such as a simplex method minimizing functional (5). After the simplex method reduces the value of a functional to a reasonably small level Newton iterations can be resumed.
(e) The tracking of a required Riemann sheet during the iterations is performed by sorting the numerically obtained eigenvalues in the decreasing order of parameter γ^R or, if it fails, by switching between the ordering procedures based on the values of σ^R and σ^I.
(f) After the saddle point location α_s is found in a complex wavenumber plane the eigenvalues are computed for a range of complex wavenumbers along the path $p \equiv \{\alpha^I = \alpha_s^I\}$. Eigenvalues forming the Riemann sheet

containing the detected saddle point are identified using one of the eigenvalue tracking procedures of step (e) and the corresponding curve $\sigma^R(p)$ is examined. If it has minima or maxima other than at α_s the iterative search is restarted at their locations to identify other saddle points which might be present on a Riemann sheet of interest.

(g) If any minima are identified at step (c) the search of branch points is initiated at their locations by minimizing the functional which is reciprocal to (5).

(h) After the saddle and branch points are located those of them with $\sigma^R > 0$ are identified. The asymptotic contribution of a branch point is computed as in [5]. The relevance of any saddle point is established by examining the images of all temporal instability branches computed at step (b) and counting the number of times the corresponding cusp point is covered by them (cusp point covered an odd number of times is a genuine pinch point). If the dominant saddle point is found to be irrelevant the next one with the second largest σ^R is examined.

(i) If the value of the absolute growth rate at the dominant saddle or branch point is nonzero the problem physical parameters are changed and all steps starting from (b) are repeated.

(j) The accurate value of physical parameters corresponding to CAIB are determined iteratively using, for example, method of chords in multi-parameter space (while similar to Newton iterations the method of chords does not require numerical Jacobian whose computations are too expensive for this purpose). The iterations stop when the value of $\left|\sigma^R\right|$ at a dominant pinch point is found to be smaller than the prescribed accuracy.

4 Concluding remarks

Although the theory of convective and absolute instabilities is well understood by now, corresponding numerical procedures remain challenging and computationally involved and frequently rely on the specifics of an individual problem. The numerical inefficiency of such procedures is mainly caused by the need for frequent human intervention i.e. visual inspection of intermediate results. Therefore it is crucial on a practical level to achieve a high degree of automatization of the complete computational process in order to enable the determination of comprehensive transition boundaries between absolute and convective instabilities in multi-parameter problems. An attempt was made here to develop such an algorithm which combines the most efficient features of individual techniques previously reported by the current and other authors. The suggested practical procedure is shown to resolve successfully the most common computational challenges of the CAIB computations some of which

could not be handled by previously known algorithms without human intervention and visual inspection. Yet it is possible that some less common situations still cannot be handled in a fully automatic way by the suggested or any other previously known procedures. For example, as discussed theoretically in [5] in addition to saddle points of $\sigma(\alpha)$ other singularities of the problem dispersion relation such as branch points or branch poles of $\sigma(\alpha)$ can contribute to the spatio-temporal behavior of a system. These were mentioned in the current paper, and a suggestion on how to find them was formulated but not tested thoroughly. The reason for this is that although a sufficiently comprehensive literature review was performed in Section 2, none of the studies cited there report such contributions in physical problems. They were not found in any of the author's own computations either and thus appear to be rare in practice. A number of other singular situations are theoretically possible. However since no physical examples where they have actually been found are reported in literature to date the author did not focus on these issues and concentrated on the development of an automatic and numerically efficient approach to comprehensive multi-parameter CAIB computations for more common situations. A comprehensive set of practical suggestions has been presented at least for the class of two-dimensional problems whose asymptotic behavior is defined by a saddle point formalism. The procedure is shown to work well in complicated physical examples. In most situations this success is warranted mathematically as demonstrated in the original studies which present individual techniques forming a foundation of the current procedure. However several cases for which no sufficient theory has yet been developed in literature are flagged and qualitative conjectures are presented instead to support the suggested numerical steps.

The proposed automatic techniques for recognizing and tracking the relevant temporal branches of the problem numerical dispersion relation can also be used for analysis of three-dimensional flows. It is also hoped that analysis of three-dimensional problems with multiple saddle points can be performed in a way similar to the one described here for two-dimensional flows (see [26] for an example of such an attempt). However the topography of Riemann sheets parameterized by two complex wavenumbers is much more diverse. Therefore the formulation of a procedure capable of catering for various possible situations in three spatial dimensions is left for the future when a sufficient number of individual three-dimensional investigations required for such a comprehensive case study are brought forward in publication.

References

[1] P. Huerre, P. A. Monkewitz, Absolute and convective instabilities in free shear layers, J. Fluid Mech. 159 (1985) 151–168.

[2] X.-Y. Yin, D.-J. Sun, M.-J. Wei, J.-Z. Wu, Absolute and convective instability character of slender viscous vortices, Phys. Fluids 12 (2000) 1062–1072.

[3] K. S. Yeo, H. Z. Zhao, B. C. Khoo, Turbulent boundary layer over a compliant surface: absolute and convective instabilities, J. Fluid Mech. 449 (2001) 141–168.

[4] K. Kupfer, A. Bers, A. K. Ram, The cusp map in the complex-frequency plane for absolute instabilities, Phys. Fluids 30 (1987) 3075–3079.

[5] L. Brevdo, A study of absolute and convective instabilities with an application to the Eady model, Geophys. Astrophys. Fluid Dyn. 40 (1988) 1–92.

[6] P. Huerre, P. A. Monkewitz, Local and global instabilities in spatially developing flows, Ann. Rev. Fluid Mech. 22 (1990) 473–537.

[7] R. J. Briggs, Electron-stream interactions with plasmas, MIT Press, Cambridge, U.S.A., 1964, Ch. 2.

[8] R. J. Lingwood, On the application of the Briggs' and steepest-descent methods to a boundary layer flow, Stud. Appl. Math. 98 (1997) 213–254.

[9] S. A. Suslov, S. Paolucci, Stability of mixed-convection flow in a tall vertical channel under non-Boussinesq conditions, J. Fluid Mech. 302 (1995) 91–115.

[10] S. A. Suslov, Searching convective/absolute instability boundary for flows with fully numerical dispersion relation, Comp. Phys. Comm. 142 (1–3) (2001) 322–325.

[11] K. S. Yeo, B. C. Khoo, H. Z. Zhao, The absolute instability of boundary-layer flow over viscoelastic walls, Theoret. Comput. Fluid Dynamics 8 (1996) 237–252.

[12] S. Jendoubi, P. J. Strykowski, Absolute and convective instability of axisymmetric jets with external flow, Phys. Fluids 6 (1994) 3000–3009.

[13] L. Krizhevsky, J. Cohen, J. Tanny, Convective and absolute instabilities of a buoyancy induced flow in thermally stratified medium, Phys. Fluids 8 (1996) 971–977.

[14] T. Loiseleux, J. M. Chomaz, P. Huerre, The effect of swirl on jets and wakes: linear instability of the Rankine vortex with axial flow, Phys. Fluids 10 (1998) 1120–1134.

[15] D. W. Lim, L. G. Redekopp, Absolute instability conditions for variable density, swirling jet flows, Eur. J. Mech., B/Fluids 17 (1998) 165–185.

[16] C. Olendraru, A. Sellier, M. Rossi, P. Huerre, Inviscid instability of Batchellor vortex: Absolute-convective transition and spatial branches, Phys. Fluids 11 (1999) 1805–1820.

[17] P. Carrière, P. A. Monkewitz, Convective versus absolute instability in mixed Rayleigh-Bénard-Poiseuille convection, J. Fluid Mech. 384 (1999) 243–262.

[18] A. Sevilla, J. M. Gordillo, C. Martinez-Bazan, The effect of the diameter ratio on the absolute and convective instability of free coflowing jets, Phys. Fluids 14 (2002) 3028–3038.

[19] R. Fernandez-Feria, C. del Pino, The onset of absolute absolute instability of rotating Hagen-Poiseuille flow: A spatial stability analysis, Phys. Fluids 14 (9) (2002) 3087–3097.

[20] R. J. Deissler, The convective nature of instability in plane Poiseuille flow, Phys. Fluids 30 (1987) 2303–2305.

[21] C. Olendraru, A. Sellier, Viscous effects in absolute-convective instability of the Batchellor vortex, J. Fluid Mech. 459 (2002) 371–396.

[22] S. A. Suslov, Effect of fluid properties variations on spatio-temporal instability of convection, in: D. Indeitsev (Ed.), Proceedings of APM2001: XXIX Summer School on "Advanced Problems in Mechanics", St Petersburg, Russia, 2001, pp. 562–569.

[23] S. A. Suslov, Spatio-temporal instabilities in mixed convection of air subject to large temperature gradient, in: D. Lyubimov (Ed.), Proceedings of the International Conference Advanced Problems in Thermal Convection, Perm, Russia, 2003.

[24] S. Suslov, Multi-mode spatiotemporal instability in non-Boussinesq convection, ANZIAM Journal (electronic), http://anziamj.austms.org.au/V45/CTAC2003, 45(E) (2004) C149–C162.

[25] L. Brevdo, Three-dimensional absolute and convective instabilities, and spatially amplifying waves in parallel shear flows, Z. angew. Math. Mech. 42 (1991) 911–942.

[26] W. Koch, On the spatio-temporal stability of primary and secondary crossflow vortices in a three-dimensional boundary layer, J. Fluid Mech. 456 (2002) 85–111.

[27] B. Pier, Finite-amplitude crossflow vortices, secondary instability and transition in the rotating-disk boundary layer, J. Fluid Mech. 487 (2003) 315–343.

[28] P. Moresco, J. J. Healey, Spatio-temporal mixed convection boundary layers, J. Fluid Mech. 402 (2000) 89–107.

[29] M. Lessen, P. J. Singh, F. Paillet, The stability of a trailing line vortex. Part 1. Inviscid theory, J. Fluid Mech. 63 (1974) 753.

[30] I. Delbende, J.-M. Chomaz, P. Huerre, Absolute/convective instabilities in the Batchelor vortex: a numerical study of the linear response, J. Fluid Mech. 355 (1998) 229–254.

[31] L. Brevdo, P. Laure, F. Dias, T. Bridges, Linear pulse structure and signalling in a film flow on an inclined plane, J. Fluid Mech. 396 (1999) 37–71.

[32] M. Ruderman, L. Brevdo, R. Erdély, Kelvin-Helmholtz absolute and convective instabilities of, and signalling in, an inviscid fluid–viscous fluid configuration, Proc. R. Soc. Lond. A 460 (2004) 847–874.

[33] T. J. Bridges, P. J. Morris, Differential eigenvalue problems in which the parameter appears nonlinearly, J. Comput. Phys. 55 (1984) 437.

[34] M. R. Khorrami, M. R. Malik, R. L. Ash, Application of spectral collocation techniques to the stability of swirling flows, J. Comp. Phys. 81 (1989) 206–229.

[35] J. Priede, G. Gerbeth, Convective, absolute, and global instabilities of thermocapillary-buoyancy convection in extended layers, Phys. Rev. E 56 (1997) 4187–4199.

[36] R. J. Deissler, Spatially growing waves, intermittency, and convective chaos in an open-flow system, Physica D 25 (1986) 233–260.

[37] C. Olendraru, A. Sellier, M. Rossi, P. Huerre, Absolute/convective instability of the Batchellor vortex, C.R. Acad. Sci. Paris/Fluid Mechanics 323 (1996) 153–159.

[38] L. Hall, W. Heckrotte, Instabilities: convective versus absolute, Phys. Rev. 166 (1968) 120–128.

[39] M. Powell, UOBYQA: unconstrained optimization by quadratic approximation, Math. Programming 92 (2002) 555–582.

[40] D. G. Duffy, Private communication, NASA/GSFC, Greenbelt, MD 20771 (2004).

[41] L. Brevdo, Convectively unstable wave packets in the Blasius boundary layer, Z. angew. Math. Mech. 75 (1995) 423–436.

[42] S. A. Suslov, Numerical aspects of determining transition to absolute instability in fluid flows, Tech. Rep. SC-MC-0203, University of Southern Queensland, Australia. http://www.sci.usq.edu.au/research/workingpapers.php (2001).